Electronic Supplementary Material (ESI) for Organic Chemistry Frontiers.

Electronic Supplementary Information

Alkylaminomaleimide Fluorophores: Synthesis via Air Oxidation and Emission Modulation by Twisted Intramolecular Charge Transfer

Yun Guo[a†], Linli Yao[a†], Ling Luo[a†], Hang-Xing Wang[a*], Ze Yang[a], Zhao Wang[a], Shu-Lun Ai[a], Yuexing Zhang[a*], Qi-Chao Zou[a] and Hao-Li Zhang[b*]

[a.] Key Laboratory for the Synthesis and Application of Organic Functional Molecules (MOE), College of Chemistry and Chemical Engineering, Hubei University, Wuhan, P.R. China, 430062, E-mail: wanghx0917@163.com; zhangyuexing@sdu.edu.cn

[b.] State Key Laboratory of Applied Organic Chemistry (SKLAOC), College of Chemistry and Chemical Engineering, Lanzhou University, Lanzhou, P.R. China, 730000, E-mail: haoli.zhang@lzu.edu.cn

Contents

Part 1. General information

Part 2. Insight into the emission

Part 3. Reaction mechanism

Part 4. Synthetic procedure

Part 5. Emission modulation

Part 6. Single crystal X-ray data

Part 7. ^{1}H-NMR, ^{13}C-NMR, and MS

References

Part 1: General information

1. Materials

All reagents as received from commercial sources were used after re-crystallization, and all solvents were used after distillation process. All experiments were carried out under air atmosphere. Column chromatographic purifications were carried out on flash silica-gel (240–400 mesh) using petroleum ether (PE) and ethyl acetate (EA) as eluents.

2. Characterizations

^{1}H NMR and ^{13}C NMR spectra were obtained on a Bruker AV-600 MHz spectrometer. ESI-MS measurements were conducted at a capillary temperature of 275 °C. Aliquots of the solution were injected into the device at 0.3 mL/h. The mass spectrometer used for the measurements was a Thermo Exactive, and the data were collected in positive ion mode. The single-crystal diffraction data were collected on a Rigaku XtaLAB synergy four-circle diffractometer with Cu-Kα radiation (λ = 1.54056 Å), with the CrysAlisPro software (version 1.171.39.34b) for data reduction and analysis. UV-Vis absorption spectra were recorded with a T6 UV/Vis Spectrometer. The photoluminescence (PL) spectra were performed using a LS55 Fluorescence Spectrometer (PerkinElmer, USA). Photographs of PL were taken using a Canon camera (EOS 550) under excitation by a hand-hold UV lamp (365 nm). Solid-state fluorescence quantum yields were measured using a Horiba JYFluorolog-3-Touspectrometer system.

3. Computational details

The molecular structures were fully optimized with B3LYP functional and 6-31G(d) basis set in chloroform solvent with the integral equation formalism polarizable

continuum model (IEFPCM) using Gaussian 16 software.[1] Harmonic-model vibrational frequencies were calculated based on the optimized geometries to verify the optimized structure to be true energy minimum. UV-vis spectroscopic calculations were made by a time-dependent (TD)-DFT method with the same method as ground state optimization based on the optimized geometry. The geometry of the first excited state was also optimized with TDDFT method to study the emission behavior. The scan for the rotation of -NR^2R^3 group along N-C bond (Figures 4 and 5) were performed by fixing the rotational angle (ϕ) and relaxing all the other structural parameters using the same method as ground state optimization. The calculated excitation energies generally corresponding well with the experimental ones, indicating the chosen method is relaible. For the present system without long π-conjugate, long-range corrected DFT method is not necessary and may get worse results. For example, long-range DFT such as M06-2X and LC-BLYP significantly overestimate the excitation energy.[2] We also certified that long-range DFT and the TRS-DFT methods only suit for long π-conjugated systems such as PBTTT.[3] As a consequence, B3LYP functional was chosen in the present work for the present system.

4. The in vitro cytotoxicity study and fluorescence imaging

The cell viability was evaluated on human epithelial cervical cancer (Hela) cells using a standard 3-(4,5-dimethylthiazol-2-yl)-2,5-diphenyltetrazolium bromide (MTT) assay.[4] Typically, HeLa cells were seeded in 96-well culture plates (1×10^4 cells/well) and incubated for 24 h at 37 ^oC. The culture medium was replaced by fresh DMEM containing various concentrations of the sequence-controlled fluorescent oligomer (noted as 11, 0-500 μg/mL) for another 24 h. Then 20 μL of MTT (5.0 mg/mL in PBS) was added into each well. After additional 4 h incubation, the growth medium was removed and 150 μL of dimethyl sulfoxide (DMSO) was added into each well to dissolve the formed formazan blue crystal. Finally, the absorbance of each sample was recorded using a microplate reader (Imark 168-1130, Biorad, USA) at a wavelength of 570 nm.

The potential for cellular imaging of the sequence-controlled fluorescent oligomer was tested in HeLa cells.[5] Typically, 2.0 mL of HeLa cells in Dulbecco's Modified Eagle Medium (DMEM) medium at an initial density of 4×10^4 cell per mL were seeded in each dish and cultured at 37 ^oC for 24 h under a humidified atmosphere containing 5% CO_2. The cells were treated with DMEM containing the oligomer (500 μg/mL) for 4 h and washed three times with PBS to remove the free sample. Finally, the samples were observed with confocal laser fluorescence microscopy.

5. Microarea PL spectra and optical waveguide measurements

To measure the PL spectra of individual microplate, the plate was excited locally with a 375 nm laser focused down to the diffraction limit. The excitation laser was filtered with a 375 nm notch filter. The light was subsequently coupled to a grating spectrometer (Princeton Instrument, ARC-SP-2356) and recorded by a thermal-electrically cooled CCD (Princeton Instruments, PIX-256E). PL microscopy images were taken with an inverted microscope (Olympus, BX43).[6]

To measure the microarea PL spectra of single microrod, the microrods dispersed on a glasscover-slip were excited with a UV laser (λ=375 nm, semiconductor laser). The excitation laser was filtered with a band-passfi lter (330–380 nm), then focused to excite the microrod with anobjective (50×, N.A. = 0.80).[7]

Part 2: Insight into the emission

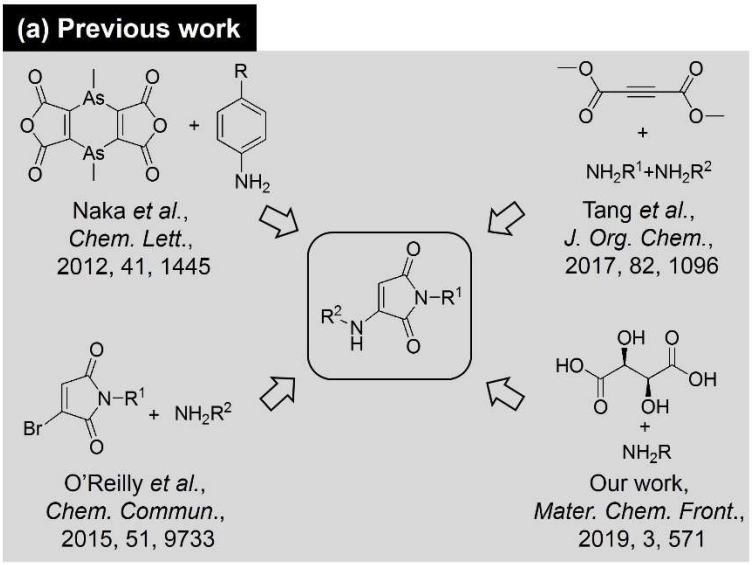

Scheme S1. (a) Previous work on synthesis of 3-aminomaleimide derivatives.

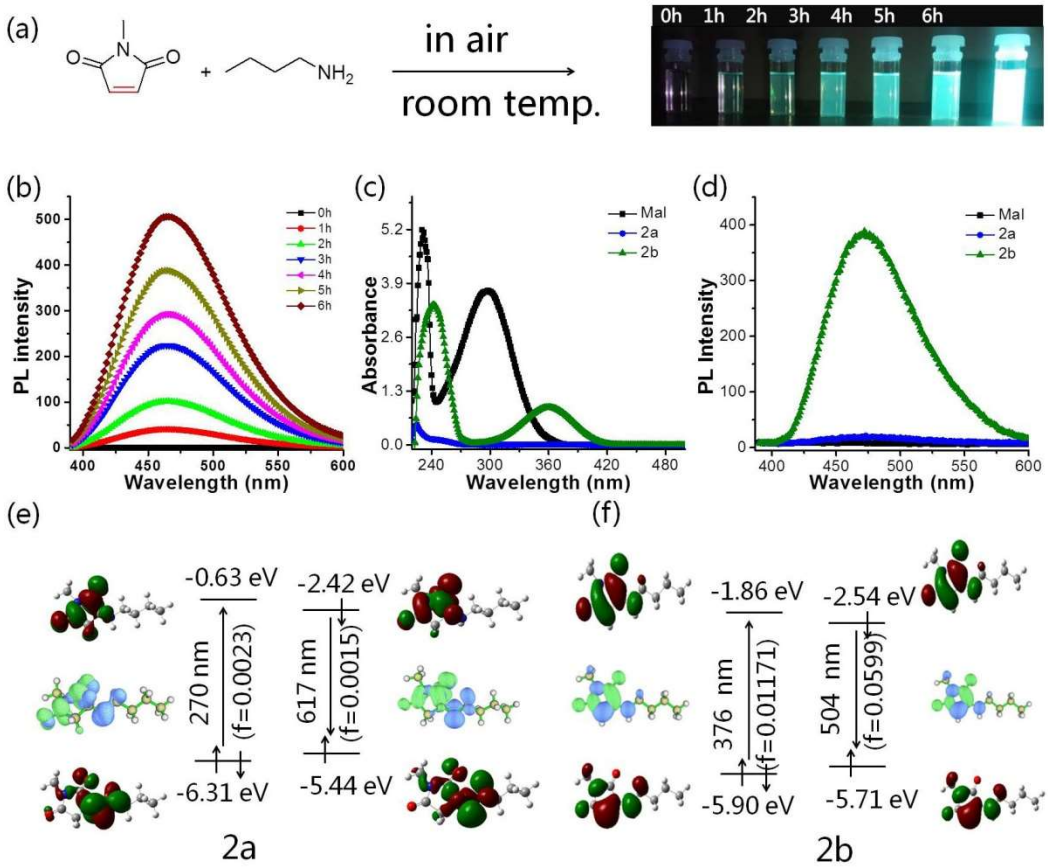

Figure S1. (a) Fluorescence from N-methyl-maleimide based Michael adduction reaction through functionalization with n-butylamine substituent. (b) PL spectra of the

Michael addition of n-butylamine to N-methyl-maleimide within 0-6 hours. (c-d) UV-Vis and PL spectra of the raw product, pure compounds of 2a and 2b. (e-f) Excitation/emission wavelength and oscillator strengths of the ground state (S_0) and first excited state (S_1) of (h) 2a and (i) 2b as determined at the (TD)DFT-B3LYP/6-31G(d) level.

Table S1. The component analysis of the Michael addition of n-butylamine to N-methyl-maleimide

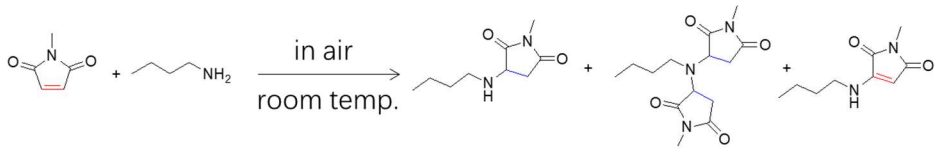

molecular formula	m/z	calc.	exp.	area ($\times 10^7$)	area (%)
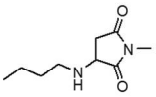	$[C_9H_{16}N_2O_2+H]^+$	185.1290	185.1270	65.9763	83.6
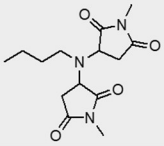	$[C_{14}H_{21}N_3O_4+H]^+$	296.1610	296.1583	10.2662	13.0
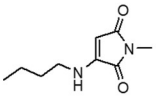	$[C_9H_{14}N_2O_2+H]^+$	183.1134	183.1117	2.7198	3.4

Noted: Yields were determined by liquid chromatography (LC)

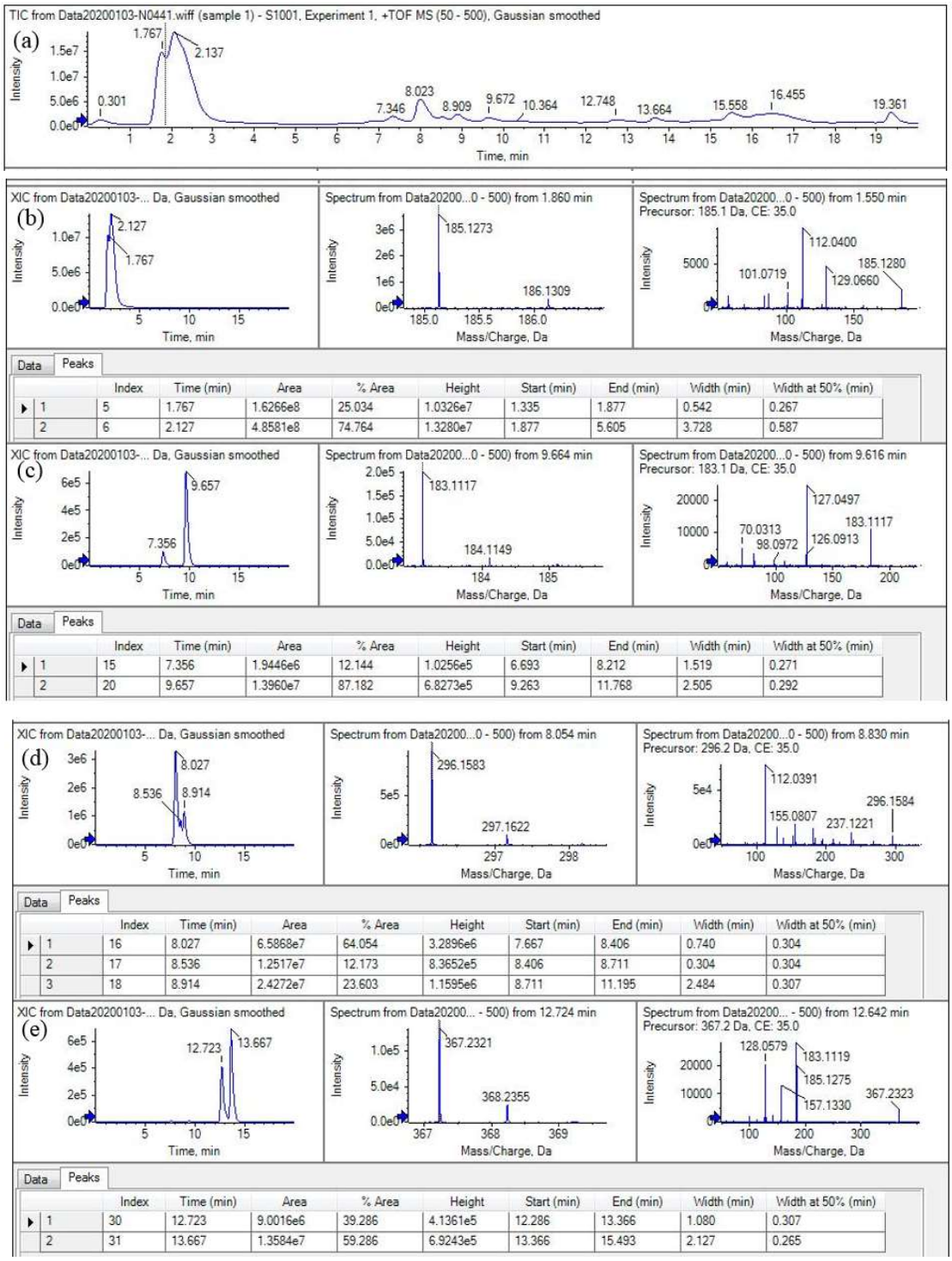

Figure S2. (a) Liquid chromatography (LC) spectrum of Michael addition product of n-butylamine to N-methyl-maleimide. (b) LC-MS of components from 1.767 min and 2.127 min. (c) LC-MS of components from 7.356 and 9.657 min. (d) LC-MS of components from 8.027 min, 8.536 min and 8.914 min. (e) LC-MS of components from 12.723 min and 13.667 min.

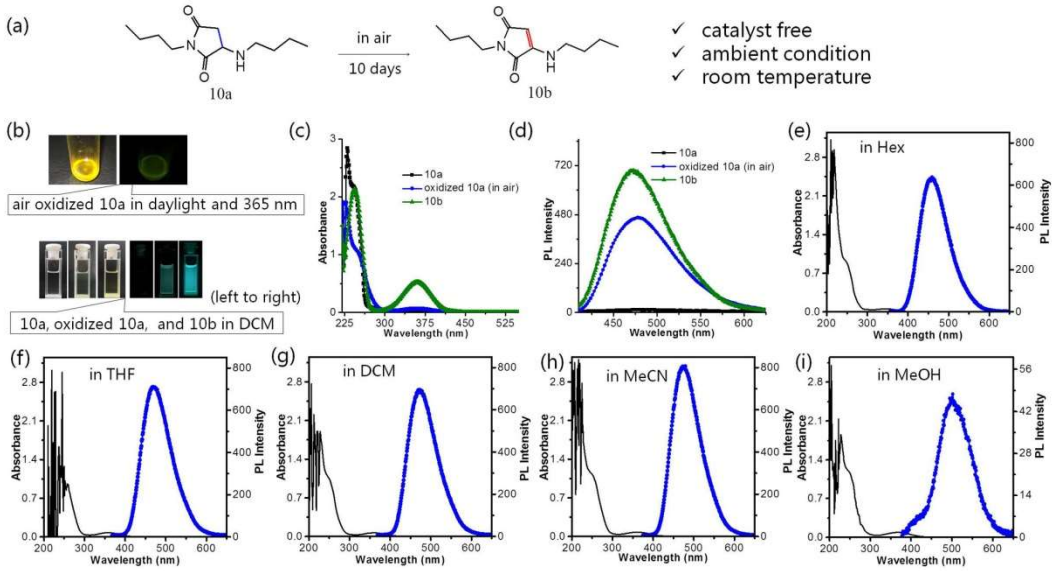

Figure S3. Fluorescence from oxidation of n-butylamine substituted succinimide (10a) under ambient condition in air. (a) Schematic diagram of 10b fluorophore from 10a via air oxidation. (b) Upper part: The images of the oily-liquid raw product under daylight and with 365 nm UV light excitation; Lower part: the images of the pure 10a, air oxidized 10a, and pure 10b under daylight and with 365 nm UV light excitation. (c-d) UV-Vis and PL spectra of the pure 10a, air oxidized 10a, and pure 10b in DCM. (e-i) UV-Vis and PL spectra of the raw in hexane (Hex), tetrahydrofuran (THF), dichloromethane (DCM), acetonitrile (MeCN), and Methanol (MeOH).

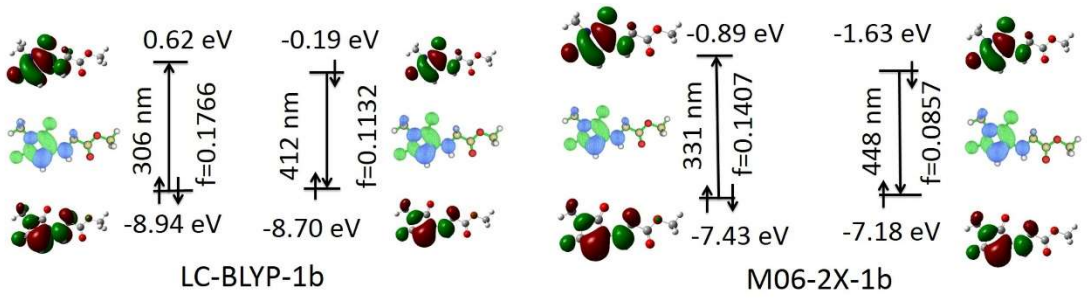

Figure S4. The excitation/emission wavelength and oscillator strengths of the ground state (S_0) and first excited state (S_1) together with the electron density difference maps between ground and excited states of 1b as determined with the LC-BLYP (top) and M06-2X (bottom) functionals using 6-31G(d) basis set.

Part 3: Reaction mechanism

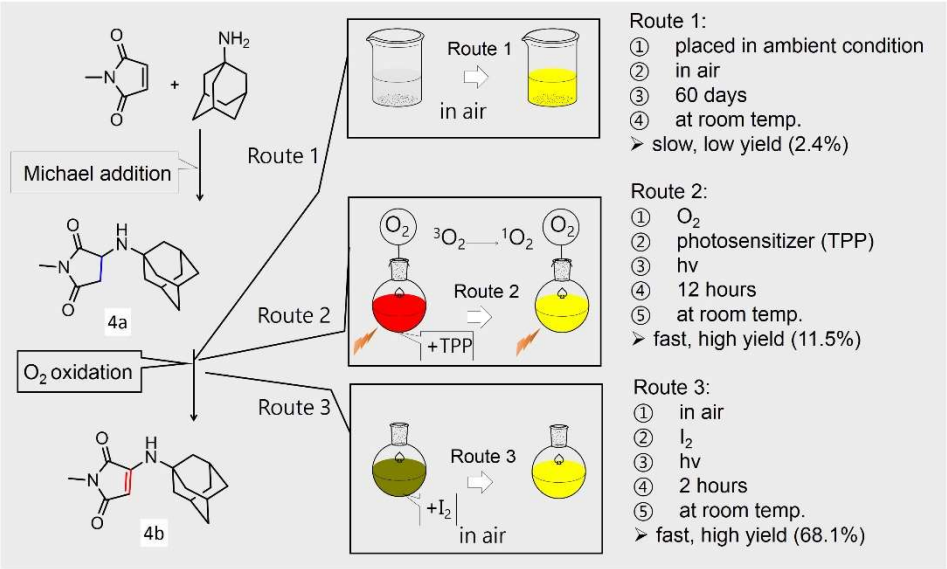

Scheme S2. Schematic diagram of synthesis of alkylaminomaleimide via Michael addition and oxidation processes in this work. The reaction yields were determined by gas chromatography-mass spectrometry (GC-MS).

Route one: Air auto-oxidation in ambient condition (see Figure S4)

In a typival procedure, the synthesized 4a as a white solid powder in a bared culture dish was directly placed in air at ambient condition for 60 days. The white solid powder slowly changed to yellow. The reactive process was monitored by thin-layer chromatography using ethylacetate (EA) and petroleumether (PE) mixed solvent, EA:PE v/v =2/3).

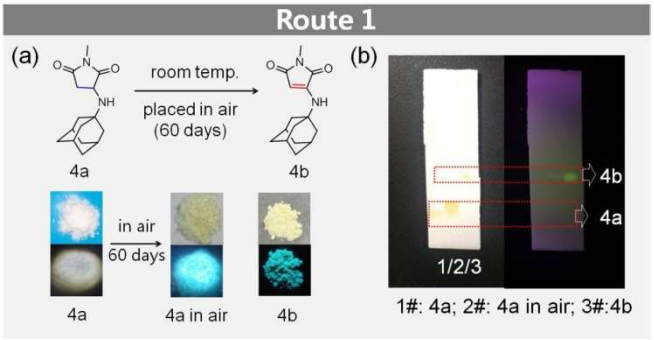

Figure S5. (a) Synthesis of 4b via air auto-oxidation. (b) The thin-layer chromatography of 4a, its corresponding air oxidation product, and 4b. (c-d) Solid-state absorption and emission spectra of 4a, its corresponding air oxidized product, and 4b.

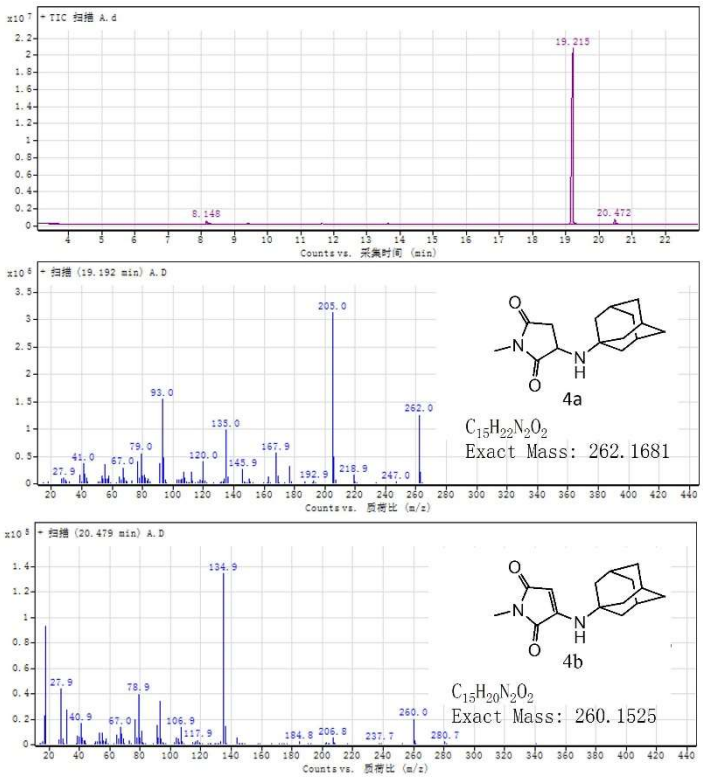

Figure S6. GC-MS spectra of 4a and 4b in route 1.

Route 2: Singlet oxygen oxidation (see Figure S6)

The precursor 4a and photosensitizer (tetraphenylporphyrin, TPP) were put into an appropriate amount of DCM solvent at a molar ratio of 100: 1, and the mixed system at room temperature under oxygen atmosphere with white LED light for 12 hours. The reactive process was monitored by thin-layer chromatography (EA: PE v/v =2/3). Finally, the mixed system was first evaporated under reduced pressure to remove the solvent. The 4b was with a yield of 11.3% as calculated by GC-MS.

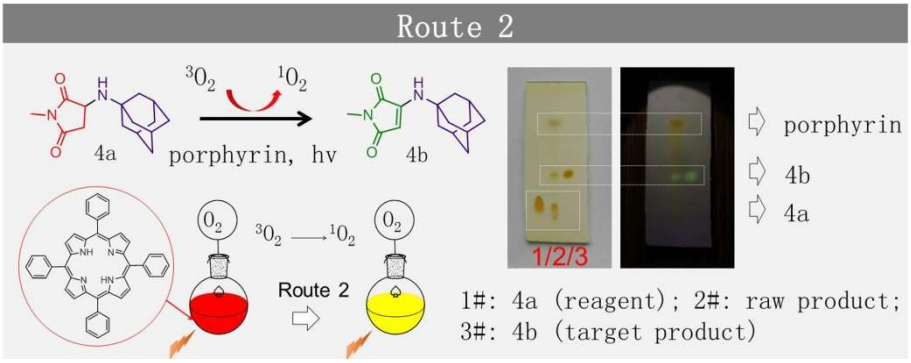

Figure S7. This work on the optimization of chemical conversion from 4a to 4b with TPP as additive.

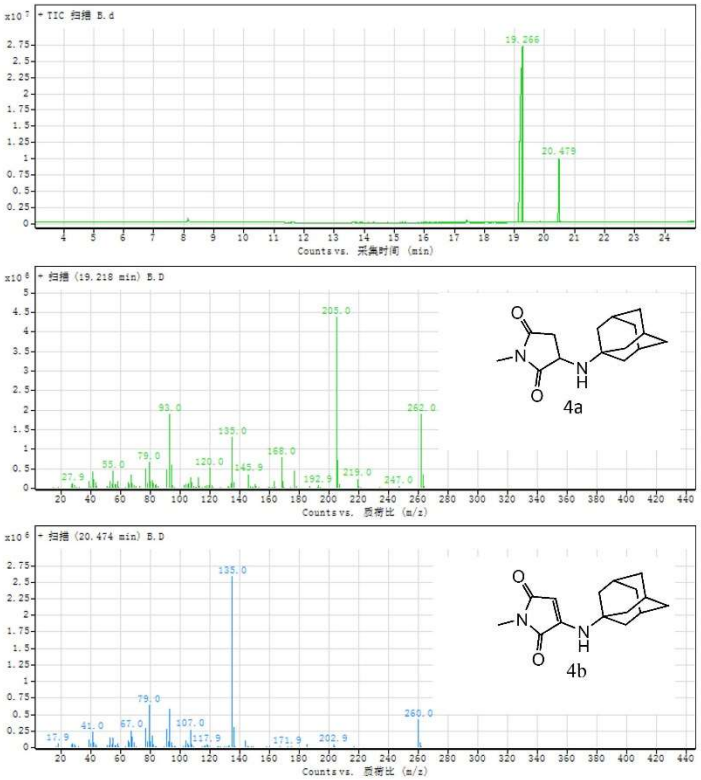

Figure S8. GC-MS spectra of 4a and 4b in route 2.

Route 3: Air oxidation with I_2 as additive (see Figure S8)

The synthesized **4a** and I_2 were put into an appropriate amount of DCM solvent at a molar ratio of 100:1, and stirred in air at room temperature for 2 hours with 500 W Xenon lamp excitation. The 4b was with a yield of 71.3% as calculated by GC-MS.

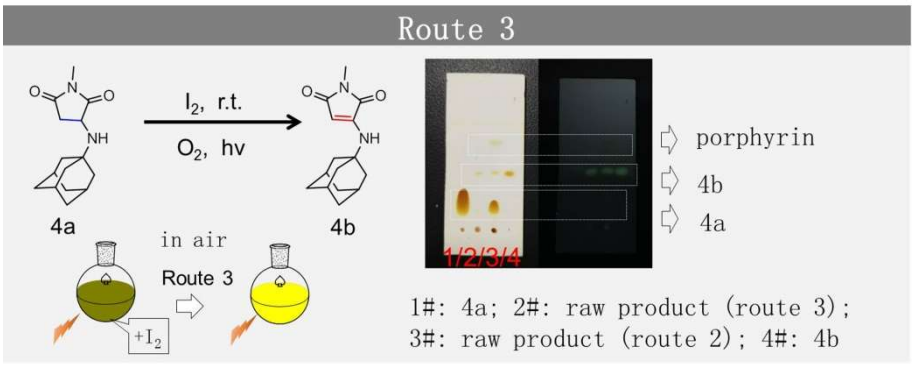

Figure S9. Synthesis of 4b via oxidation using I_2 as an additive.

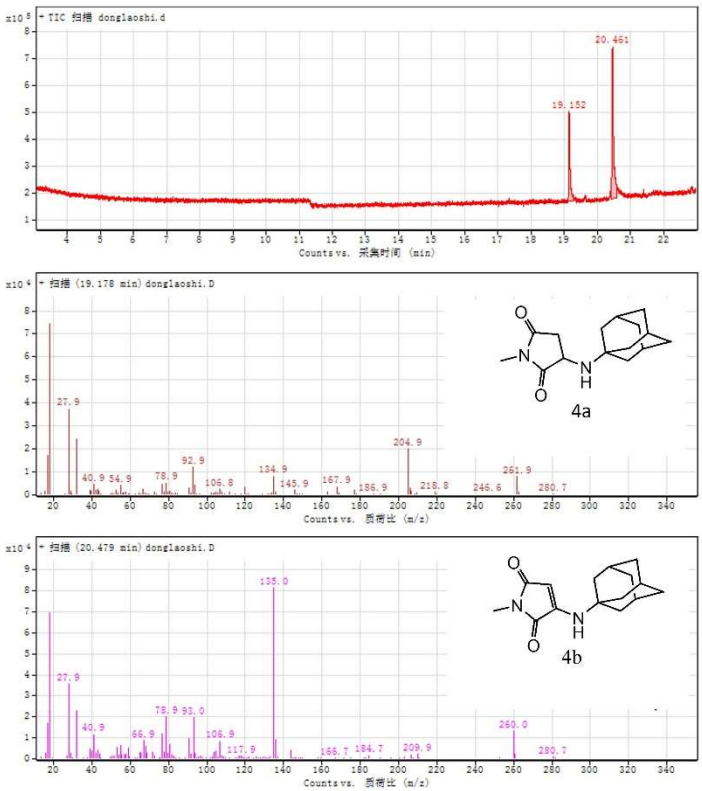

Figure S10. GC-MS spectra of 4a and 4b in route 3.

Table S2. Component analysis of three route prepared 4b by GC-MS.

sample	peak	RT	area	area(%)	peak height	sum of peak areas(%)	labeling (target compound)
4a-4b (route 1)	1	19.215	69645968.65	100	20565283.83	97.6	4a
	2	20.472	1716934.56	2.47	559283.82	2.4	4b
4a-4b (route 2)	1	19.245	110056235.3	100	25740174.05	66.7	4a
	2	19.266	35977231.34	32.69	27016856.49	21.8	TPP
	3	20.479	18905629.03	17.18	9856233.4	11.5	4b
4a-4b (route 3)	1	19.152	920784.98	46.75	333662.65	31.9	4a
	2	20.461	1969633.15	100	564684.37	68.1	4b

Part 4: Synthetic procedure

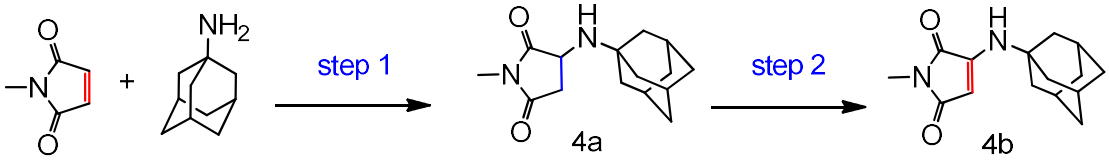

Scheme S3. Synthetic route of primary alkyl amine substituted maleimide derivatives by chosen 4a and 4b as model compounds.

Step 1: Maleimide-based Michael addition reaction was used to synthesize 4a.[8]

In a typival procedure, N-methy-maleimide (1.11 g, 10 mmol) of dissolved in 50 mL of methol (MeOH) was added dropwise tricyclo[3.3.1.$1^{3,7}$]decan-1-amine (10 mmol) dissolved in 15 mL of MeOH. Finally, the resulting reaction mixture was stirred at room temperature for 12 h. After completion, the solvent was removed under reduced pressure and the crude product was extracted with ethyl acetate and then washed with sodium hydrogen carbonate solusion, water and brine, respectively. After drying with magnesium sulfate, the crude maleimide adduct was purified by silica-gel column chromatography with n-hexane and ethyl acetate as an eluent to afford **4a** as a white solid powder with a yield of 74.5%.

Step 2: Chemical conversion 4a to 5b via air oxidation

The synthesized **4a** and I_2 were put into an appropriate amount of DCM solvent at a molar ratio of 100:1, and stirred in air at room temperature for 2 hours with 500 W Xenon lamp excitation. The solvent was first evaporated under reduced pressure and the crude product was extracted with ethyl acetate and then washed with sodium hydrogen carbonate solusion, water and brine, respectively. After drying with magnesium sulfate, the crude maleimide adduct was purified by silica-gel column chromatography with EA:PE (v/v=2/3) as an eluent to afford **4b** as a yellow solid powder.

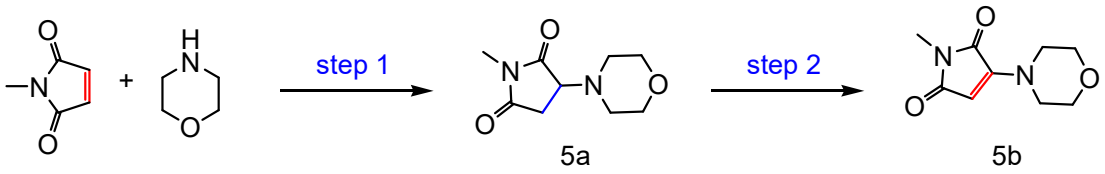

Scheme S4. Synthetic route of secondary alkyl amine substituted maleimide derivatives by chosen 5a and 5b as model compounds.

Step 1: Maleimide-based Michael addition reaction was used to synthesize 5a.[8]

In a typival procedure, N-methy-maleimide (1.11 g, 10 mmol) of dissolved in 50 mL of methol (MeOH) was added dropwise morpholine (10 mmol) dissolved in 15 mL of DCM. Finally, the resulting reaction mixture was stirred at room temperature for 12 h. After completion, the solvent was removed under reduced pressure and the crude product was extracted with ethyl acetate and then washed with sodium hydrogen carbonate solusion, water and brine, respectively. After drying with magnesium sulfate, the crude maleimide adduct was purified by silica-gel column chromatography with n-hexane and ethyl acetate as an eluent to afford **5a** as a white solid powder with a yield of 60.1%.

Step 2: Chemical conversion 5a to 5b via air oxidation

The synthesized **5a** and I_2 were put into an appropriate amount of DCM solvent at a molar ratio of 100:1, and stirred in air at room temperature for 2 hours with 500 W Xenon lamp excitation. The solvent was first evaporated under reduced pressure and the crude product was extracted with ethyl acetate and then washed with sodium hydrogen carbonate solusion, water and brine, respectively. After drying with magnesium sulfate, the crude maleimide adduct was purified by silica-gel column chromatography with EA:PE (v/v=1/1) as an eluent to afford **5b** as a yellow solid powder.

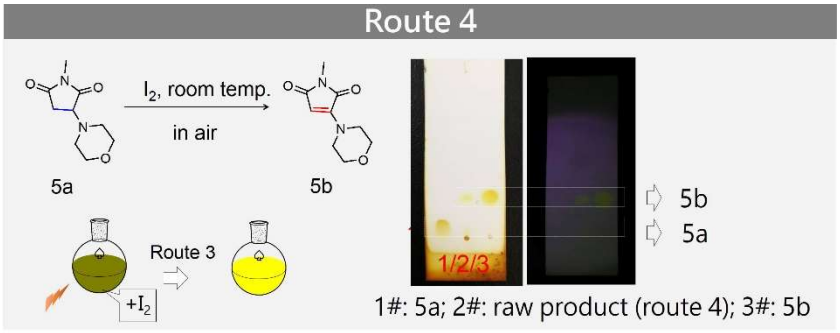

Figure S11. Synthesis of 5b via oxidation using I_2 as an additive.

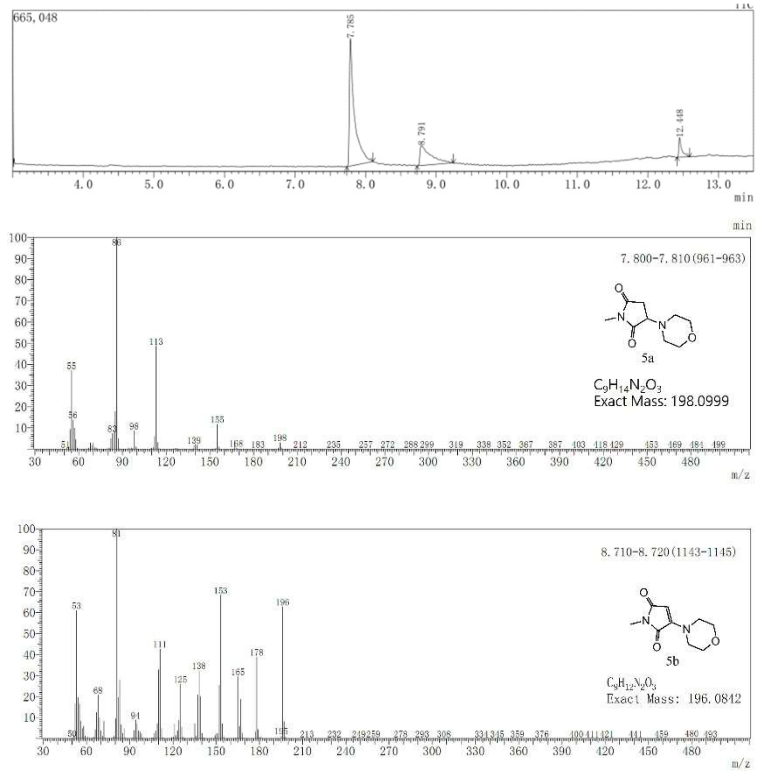

Figure S12. GC-MS spectra of 5a and 5b in route 4.

Table S3. Component analysis of prepared 5b via oxidation using I_2 as an additive (route 4) by GC-MS.

sample	peak	RT	area	area(%)	peak height	sum of peak areas(%)	labeling (target compound)
5a-5b (route 3)	1	7.785	2609741	100	527900	74.6	5a
	2	8.791	886744	33.98	82468	25.4	5b

Part 5: Accurate modulation of emission

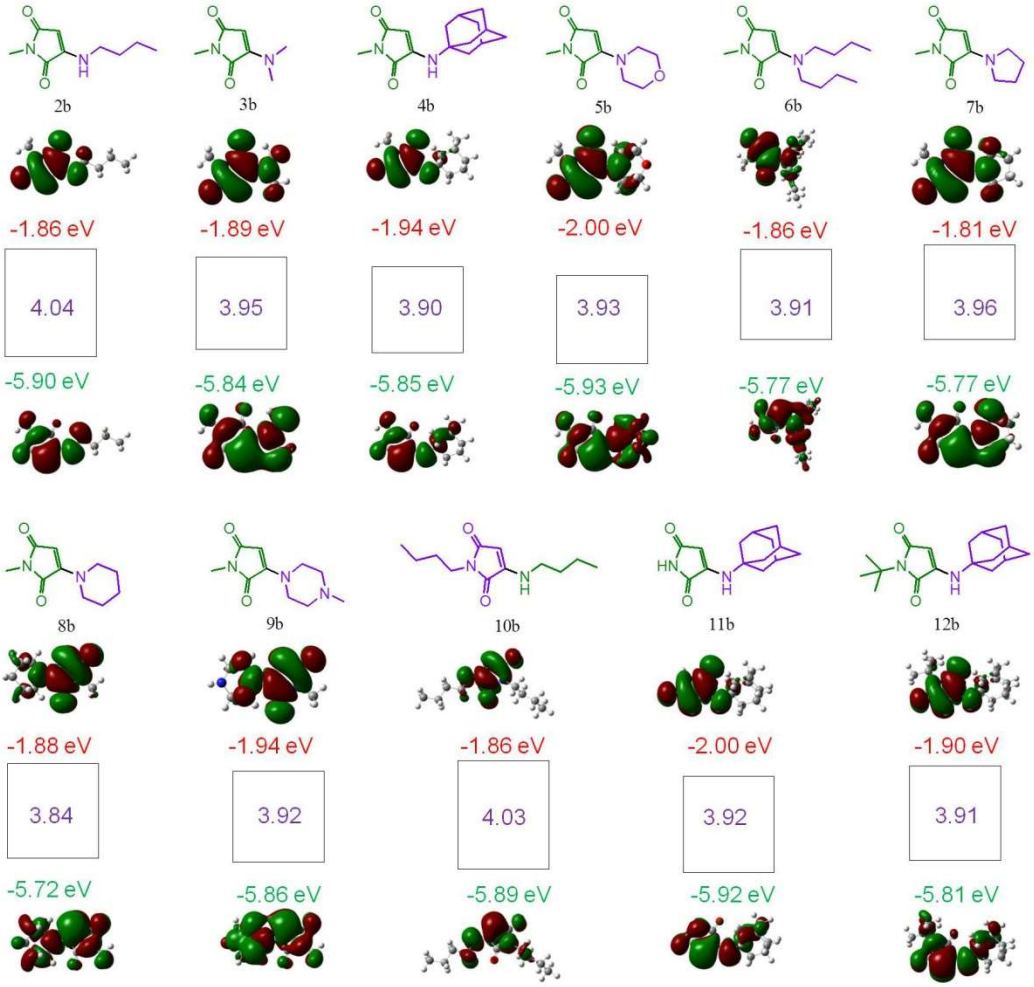

Figure S13. HOMO, LUMO and energy gap of compounds 2b-12b.

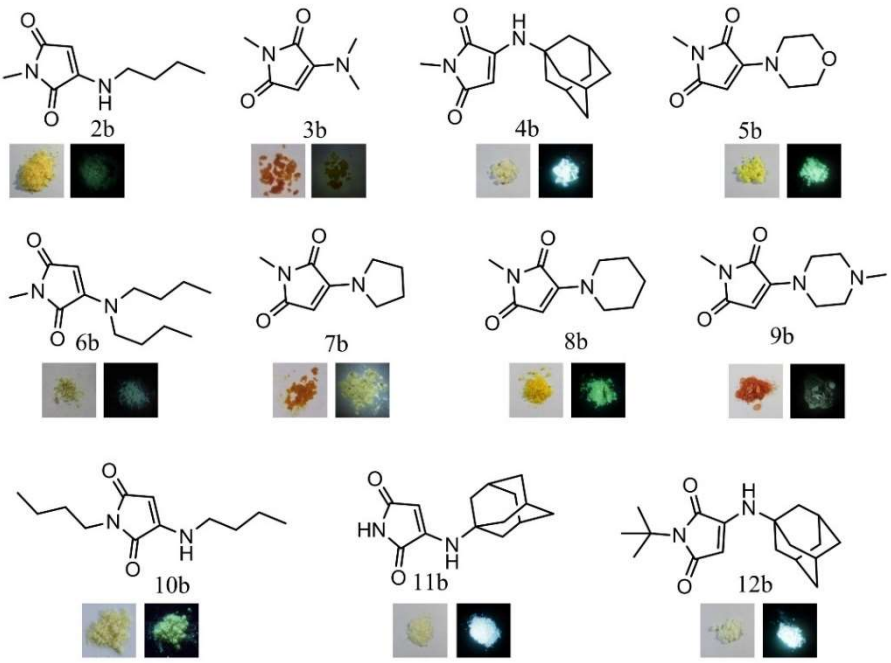

Figure S14. The molecular structures, digital images in daylight and with 365 nm excitation of the 3-alkylamniomaleimide compounds 2b-12b.

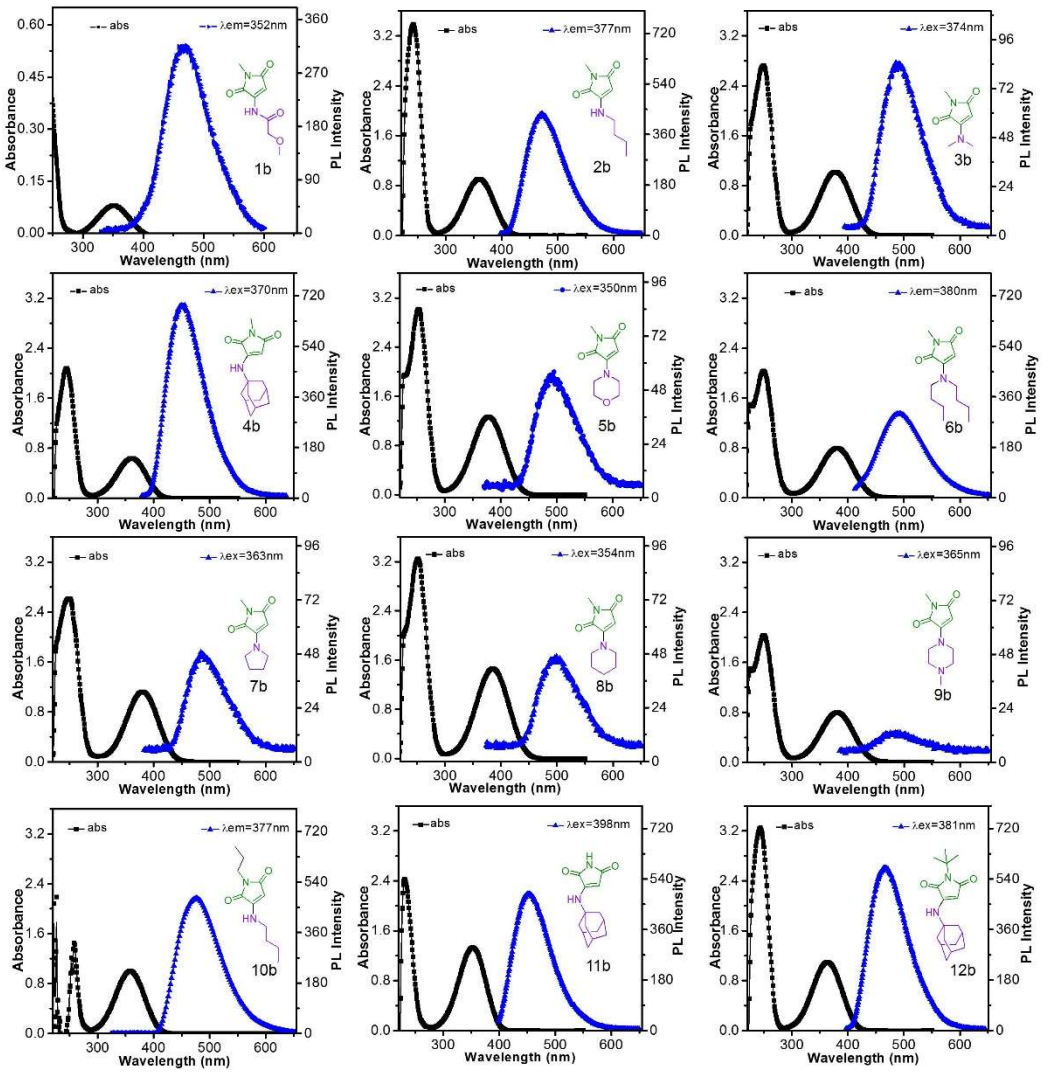

Figure S15. UV-Via and PL spectra of compounds 1b-12b in DCM.

Noted: All the PL spectra of solution samples are measured in dilute solution without observing aggregation in solution.

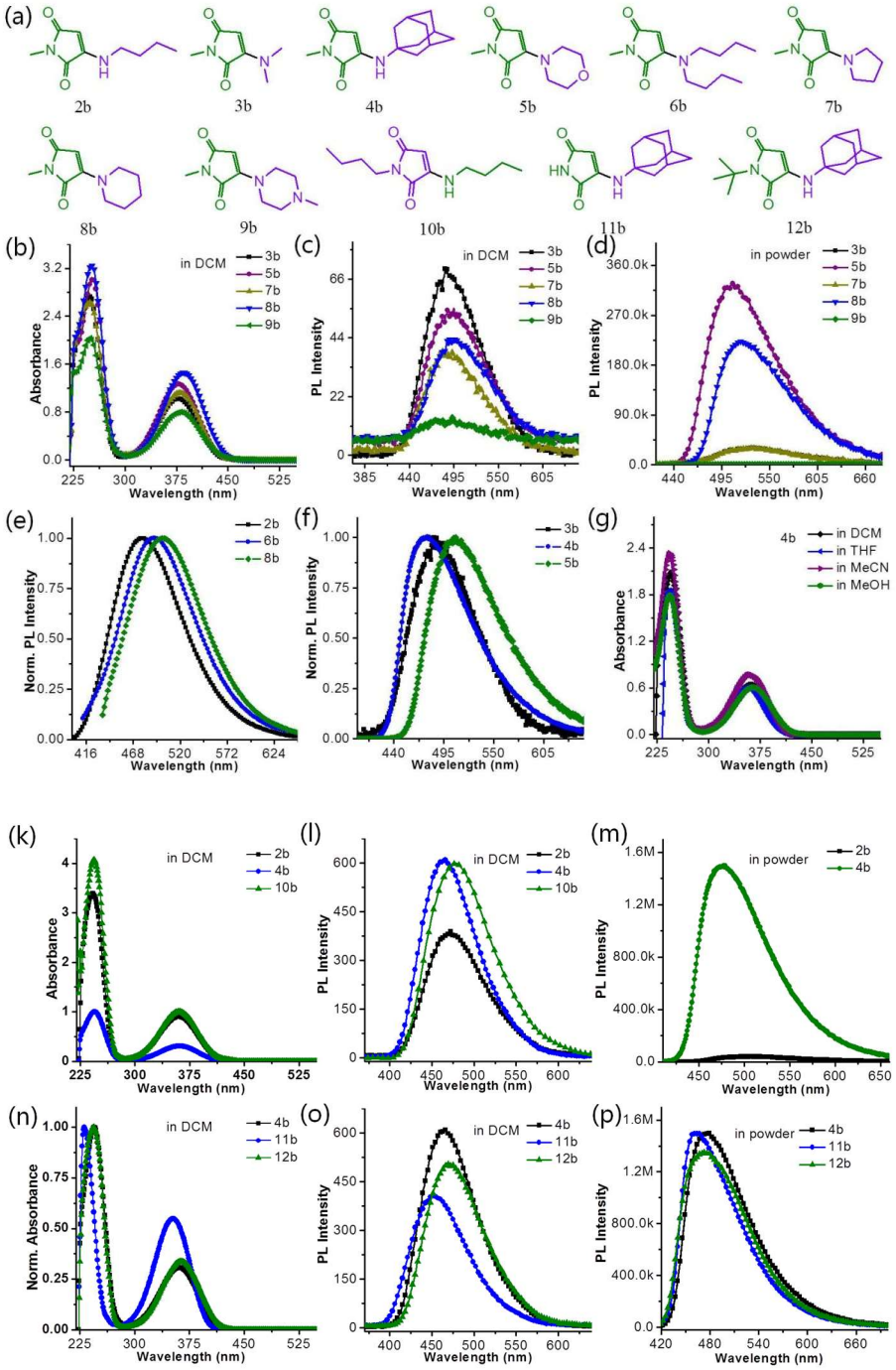

Figure S16. UV-Vis and PL spectra of different amino group substituted maleimide derivatives.

Noted: All the PL spectra of solution samples are measured in dilute solution without observing aggregation in solution. Solid-state PL spectra of 3-aminomaleimide compounds were obtained from the powder measurements.

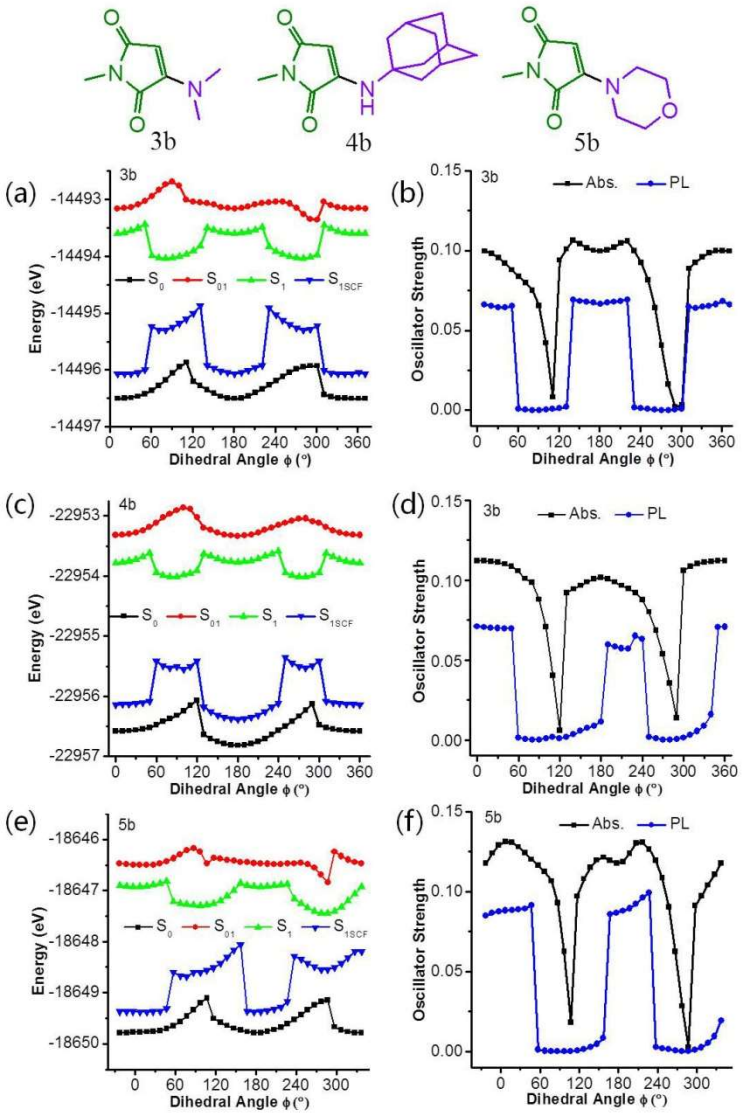

Figure S17. Energy levels of the ground and excited states of compounds 3b, 4b, and 5b with variable dihedral angles ϕ calculated at the TD/B3LYP/6-31G(d) level. Oscillator strength changes in the first electronic transition S_0-S_1 and S_1-S_0 by the rotation.

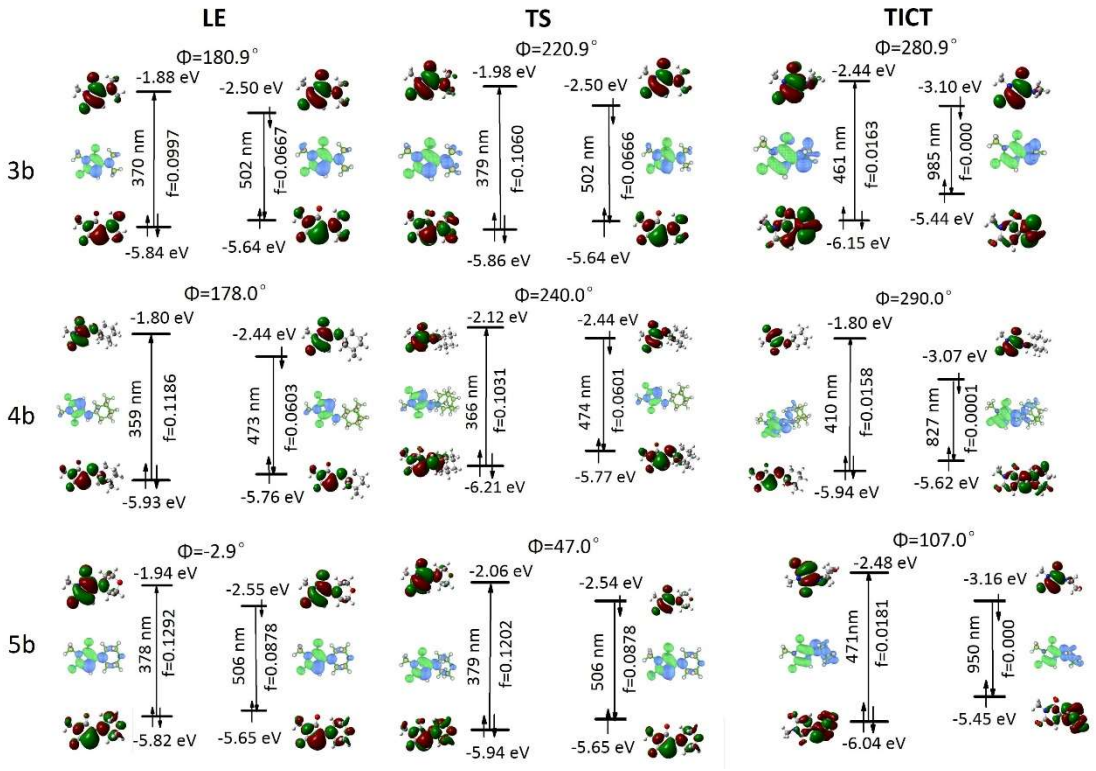

Figure S18. The excitation/emission wavelength and oscillator strengths of the ground state (S_0) and first excited state (S_1) together with the electron density difference maps between ground and excited states of 3b (top), 4b (middle), and 5b (bottom) at three different rotational angle (ϕ) corresponding to LE (left), TS (middle), and TICT (right) states, respectively, as determined at the B3LYP/6-31G(d) level.

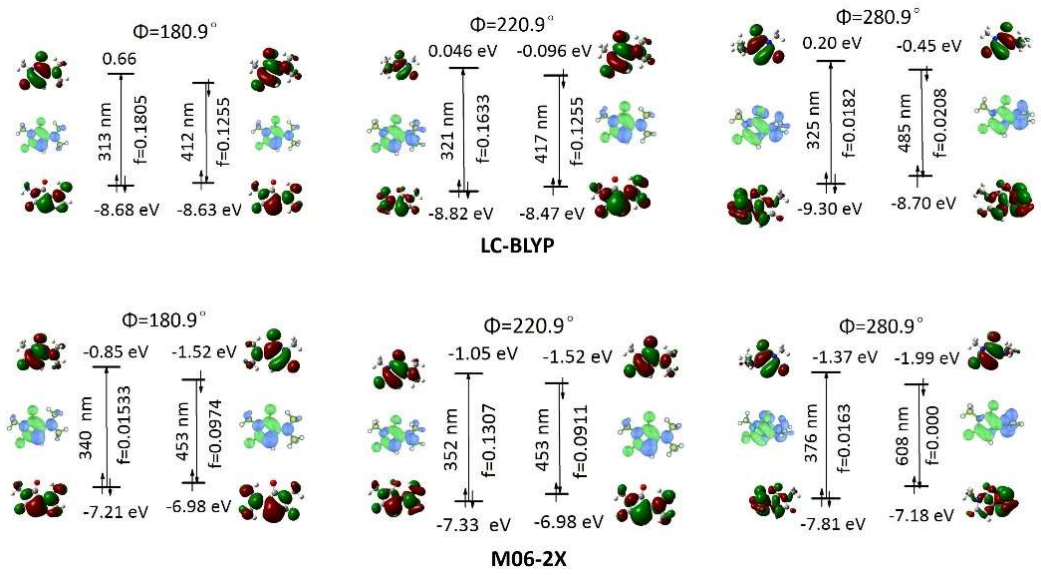

Figure S19. The excitation/emission wavelength and oscillator strengths of the ground state (S_0) and first excited state (S_1) together with the electron density difference maps between ground and excited states of 3b at three different rotational angle (ϕ) corresponding to LE (left), TS (middle), and TICT (right) states, respectively, as determined with the LC-BLYP (top) and M06-2X (bottom) functionals using 6-31G(d) basis set.

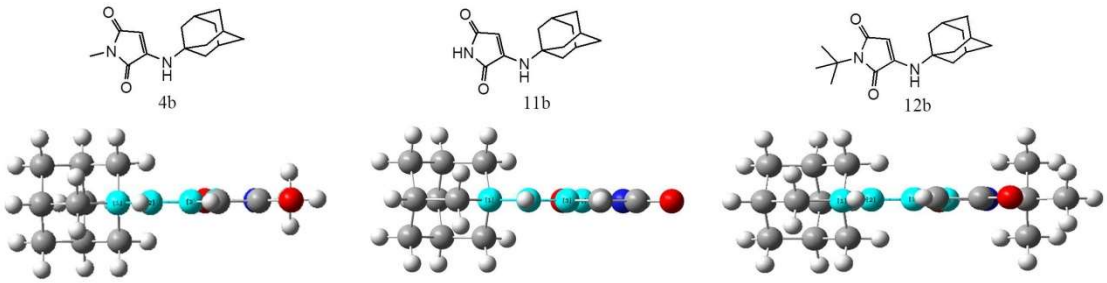

Figure S20. Top view of the theoretically optimized molecular structures of 4b, 11b, and 12b in the ground state.

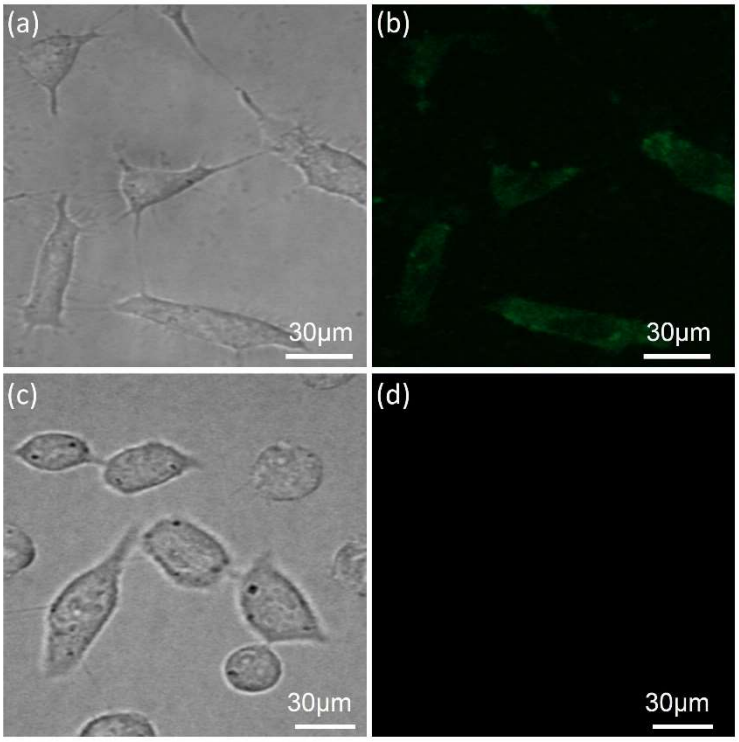

Figure S21. Cellular imaging of the sequence-controlled fluorescent oligomer tested in HeLa cells. Bright-field image and confocal fluorescent images of HeLa cells incubated with the fluorescent oligomer (a-b) and without treatment of the fluorescent oligomer (c-d).

Part 6: Single crystal X-ray data

Table S4. Crystal data and structure refinement for 4a

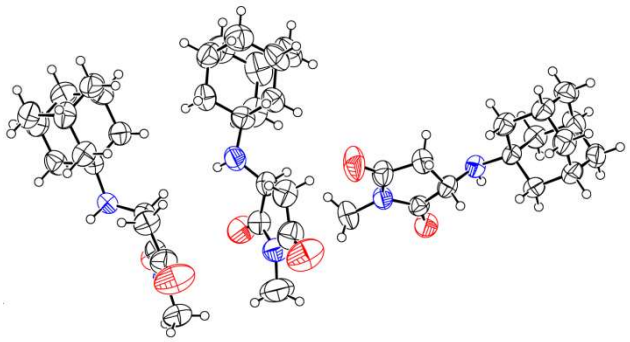

Identification code	4a
Empirical formula	$C_{15}H_{22}N_2O_2$
Formula weight	262.01
Temperature/K	293(2)
Crystal system	triclinic
Space group	P-1
a/Å	6.70980(10)
b/Å	16.3450(4)
c/Å	20.5918(4)
α/°	109.695(2)
β/°	90.2440(10)
γ/°	97.475(2)
Volume/Å^3	2105.35(8)
Z	6
ρ_{calc}g/cm^3	1.240
μ/mm^{-1}	0.660
F(000)	850.0
Crystal size/mm^3	0.15 × 0.1 × 0.08
Radiation	CuKα (λ = 1.54184)
2Θ range for data collection/°	5.8 to 148.652
Index ranges	-7 ≤ h ≤ 8, -19 ≤ k ≤ 19, -25 ≤ l ≤ 25
Reflections collected	14329
Independent reflections	14329 [Rint = ?, Rsigma = 0.0101]
Data/restraints/parameters	14329/0/524
Goodness-of-fit on F^2	1.050
Final R indexes [I>=2σ (I)]	R_1 = 0.0869, wR_2 = 0.2628
Final R indexes [all data]	R_1 = 0.0929, wR_2 = 0.2715
Largest diff. peak/hole / e Å^{-3}	0.50/-0.38

Table S5. Crystal data and structure refinement for 4b

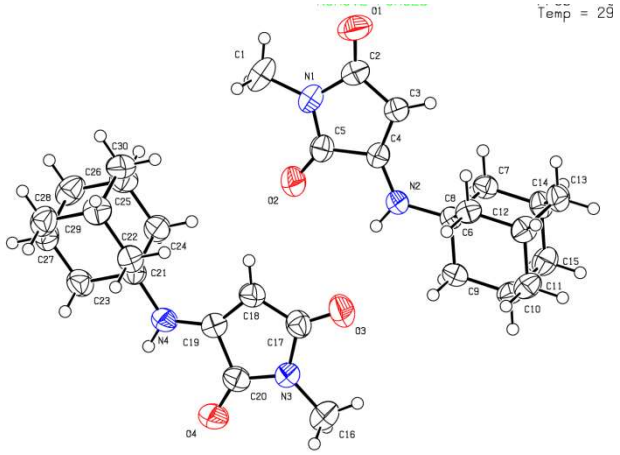

Identification code	4b
Empirical formula	$C_{30}H_{40}N_4O_4$
Formula weight	520.66
Temperature/K	293(2)
Crystal system	monoclinic
Space group	P21/n
a/Å	12.6504(2)
b/Å	9.88430(10)
c/Å	21.2340(3)
α/°	90
β/°	91.5550(10)
γ/°	90
Volume/Å^3	2654.13(6)
Z	4
ρ_{calc}g/cm^3	1.303
μ/mm^{-1}	0.698
F(000)	1120.0
Crystal size/mm^3	0.1 × 0.08 × 0.05
Radiation	CuKα (λ = 1.54184)
2Θ range for data collection/°	8.04 to 134.98
Index ranges	-15 ≤ h ≤ 15, -11 ≤ k ≤ 10, -24 ≤ l ≤ 25
Reflections collected	29368
Independent reflections	4772 [Rint = 0.0321, Rsigma = 0.0178]
Data/restraints/parameters	4772/0/345
Goodness-of-fit on F^2	1.068
Final R indexes [I>=2σ (I)]	R_1 = 0.0580, wR_2 = 0.1790
Final R indexes [all data]	R_1 = 0.0629, wR_2 = 0.1848
Largest diff. peak/hole / e Å^{-3}	0.57/-0.22

Part 7: ^{1}H-NMR, ^{13}C-NMR, and MS

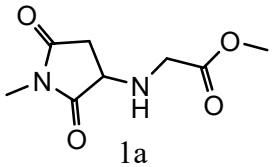

1a

1a: ^{1}H NMR (501 MHz, $CDCl_3$, ppm): δ 3.82 (dd, *J* = 8.3, 4.8 Hz, 1H), 3.74 (s, 3H), 3.59 (q, *J* = 17.4 Hz, 2H), 2.98 (s, 3H), 2.52 (dd, *J* = 18.0, 4.6 Hz, 2H), ^{13}C NMR (126 MHz, $CDCl_3$, ppm): δ 177.38, 174.96, 171.94, 77.38, 77.12, 76.87, 55.27, 52.04, 48.39, 36.12, 24.75. ESI-MS for **1a**, $[M+CH_3OH+Na]^+$ Calcd: m/z = 255.0951; Found: 255.0941.

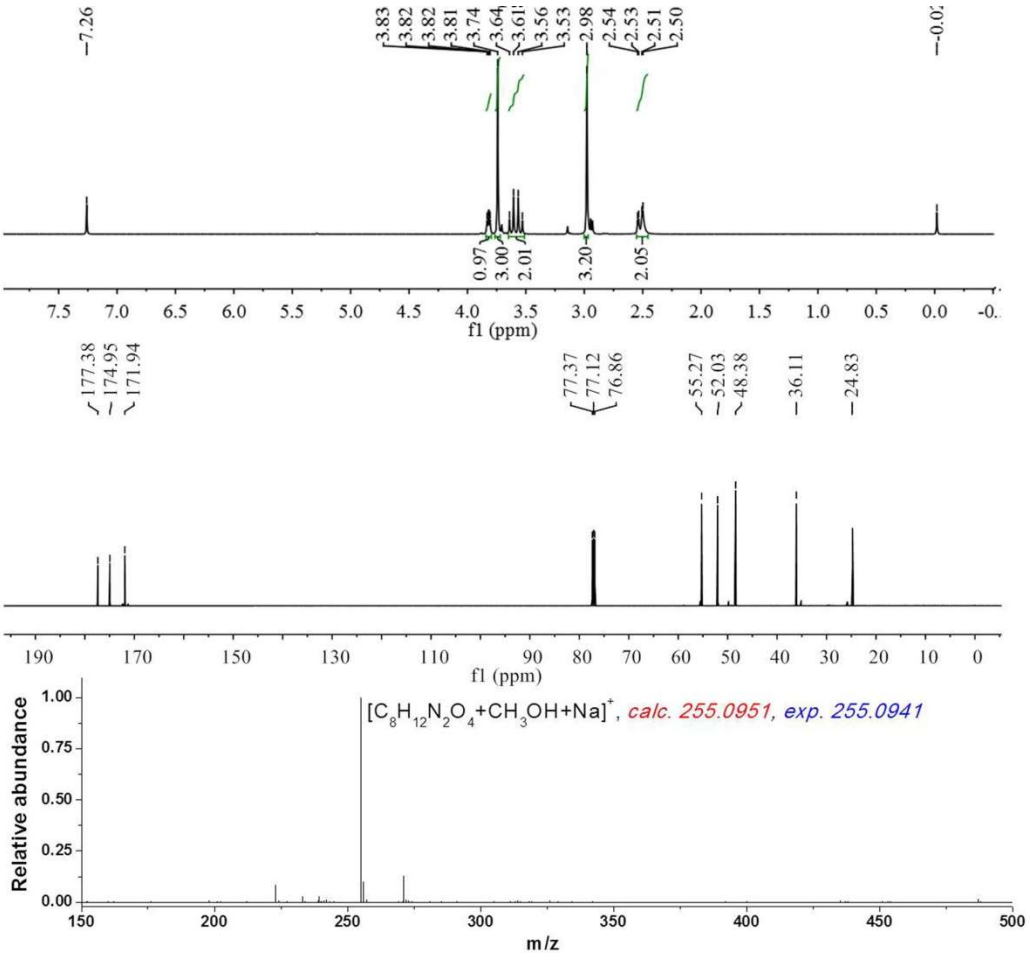

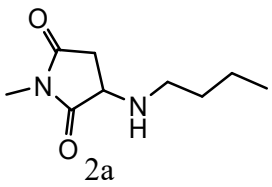

2a

2a: ^{1}H NMR (501 MHz, $CDCl_3$, ppm): δ 3.74 – 3.64 (m, 1H), 2.92 (s, 3H), 2.86 (dd, J = 18.1, 7.7 Hz, 1H), 2.62 (d, J = 7.1 Hz, 1H), 2.49 (dd, J = 32.3, 12.5 Hz, 2H), 1.86 (s, 1H), 1.42 (d, J = 6.0 Hz, 2H), 1.30 (d, J = 7.1 Hz, 2H), 0.85 (t, J = 6.8 Hz, 3H), ^{13}C NMR (126 MHz, $CDCl_3$, ppm): δ 178.09, 175.51, 56.47, 47.44, 36.10, 32.09, 24.75, 20.29, 13.91. ESI-MS for **2a**, $[M+H]^+$Calcd: m/z = 185.1285; Found: 185.1278.

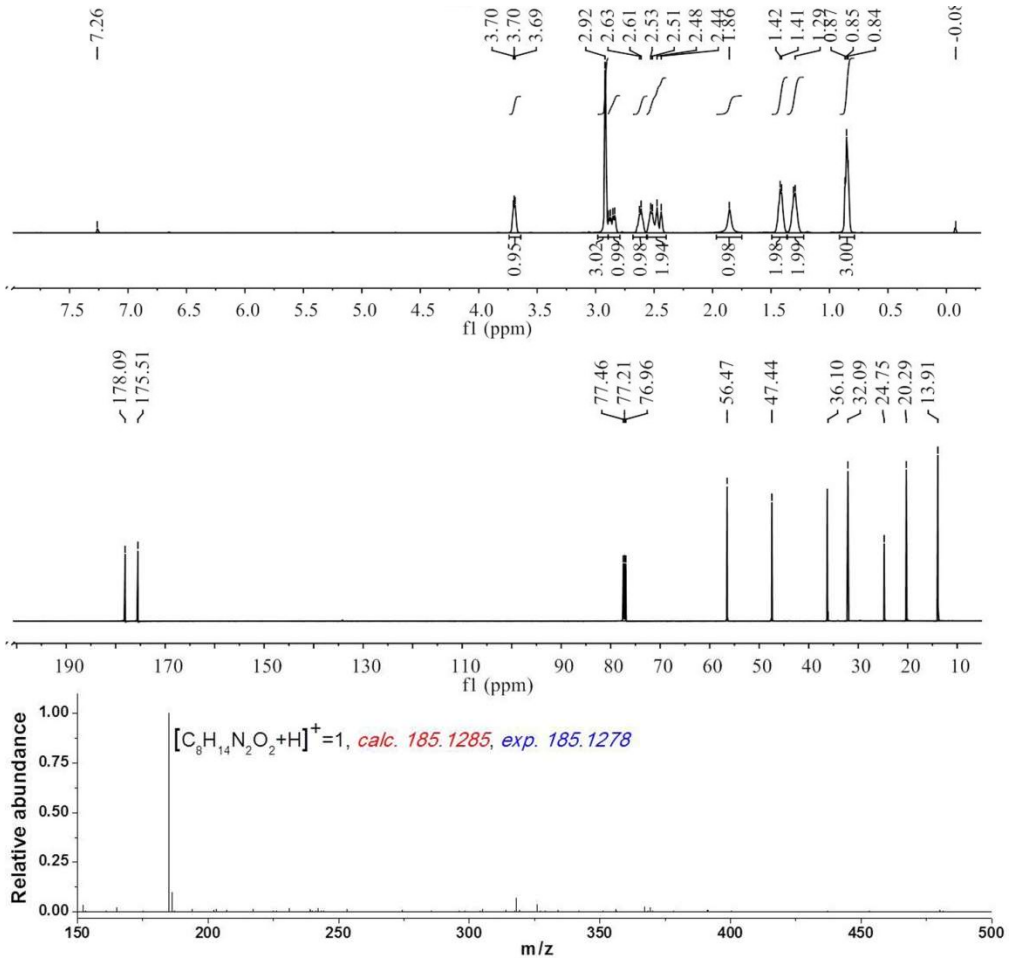

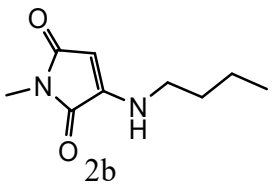

2b

2b: ^{1}H NMR (400 MHz, $CDCl_3$, ppm): δ 5.37 (s, 1H), 4.79 (s, 1H), 3.16 (dd, J = 13.1, 7.0 Hz, 2H), 2.96 (s, 3H), 1.66 – 1.57 (m, 2H), 1.39 (dq, J = 14.6, 7.3 Hz, 2H), 0.94 (t, J = 7.3 Hz, 3H), ^{13}C NMR (101 MHz, $CDCl_3$, ppm): δ 172.69, 167.66, 149.49, 83.83, 44.01, 30.55, 23.45, 20.00, 13.66. ESI-MS for **2b**,$[M+H]^+$ Calcd: m/z = 183.1128; Found: 183.1121; $[M+Na]^+$ Calcd: m/z = 205.0947; Found: 205.0942.

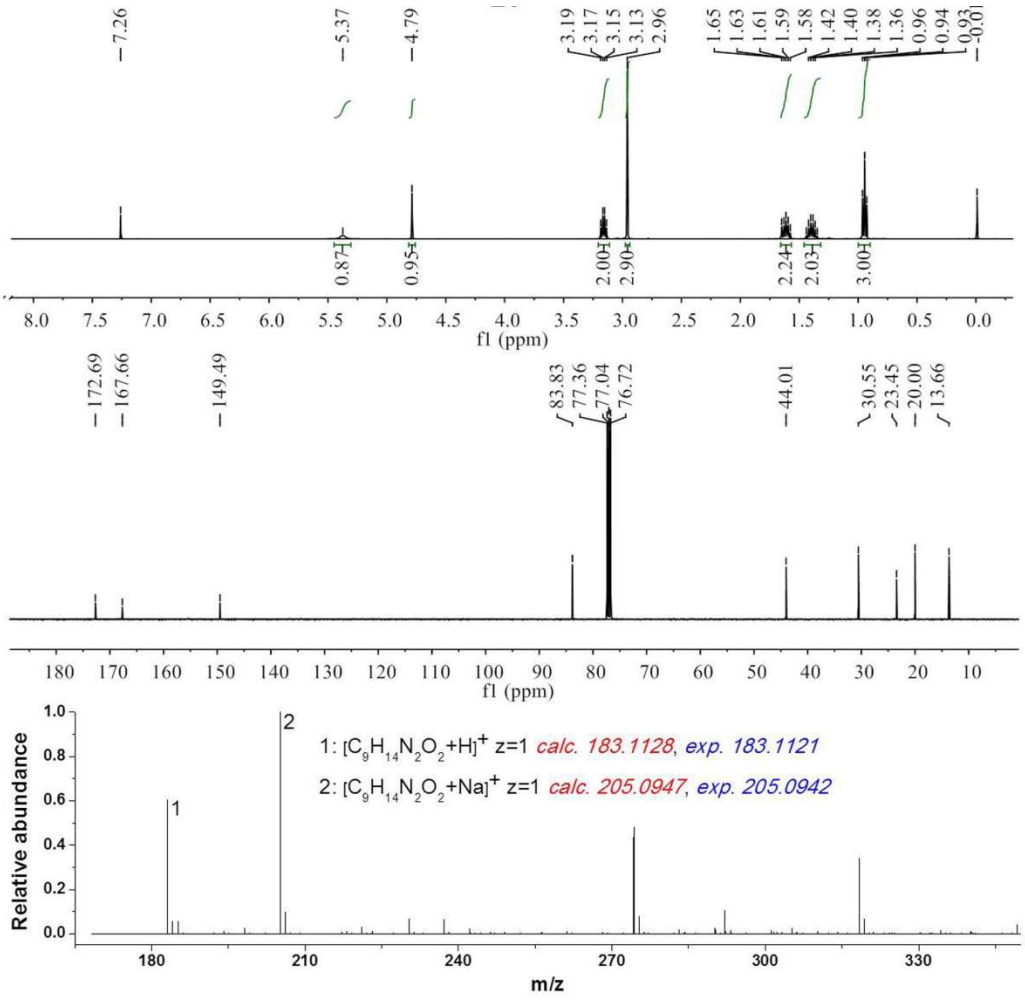

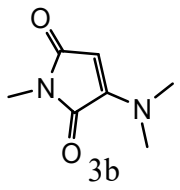

3b

3b: ^{1}H NMR (400 MHz, $CDCl_3$, ppm): δ 4.74 (s, 1H), 3.15 (s, 6H), 2.89 (s, 3H), ^{13}C NMR (101 MHz, $CDCl_3$, ppm): δ 171.09, 166.99, 150.99, 87.16, 60.36, 23.27, -0.02. ESI-MS for **3b**,$[M+H]^+$ Calcd: m/z = 155.0815; Found: 155.1176; $[M+Na]^+$ Calcd: m/z = 177.0634; Found: 177.1004.

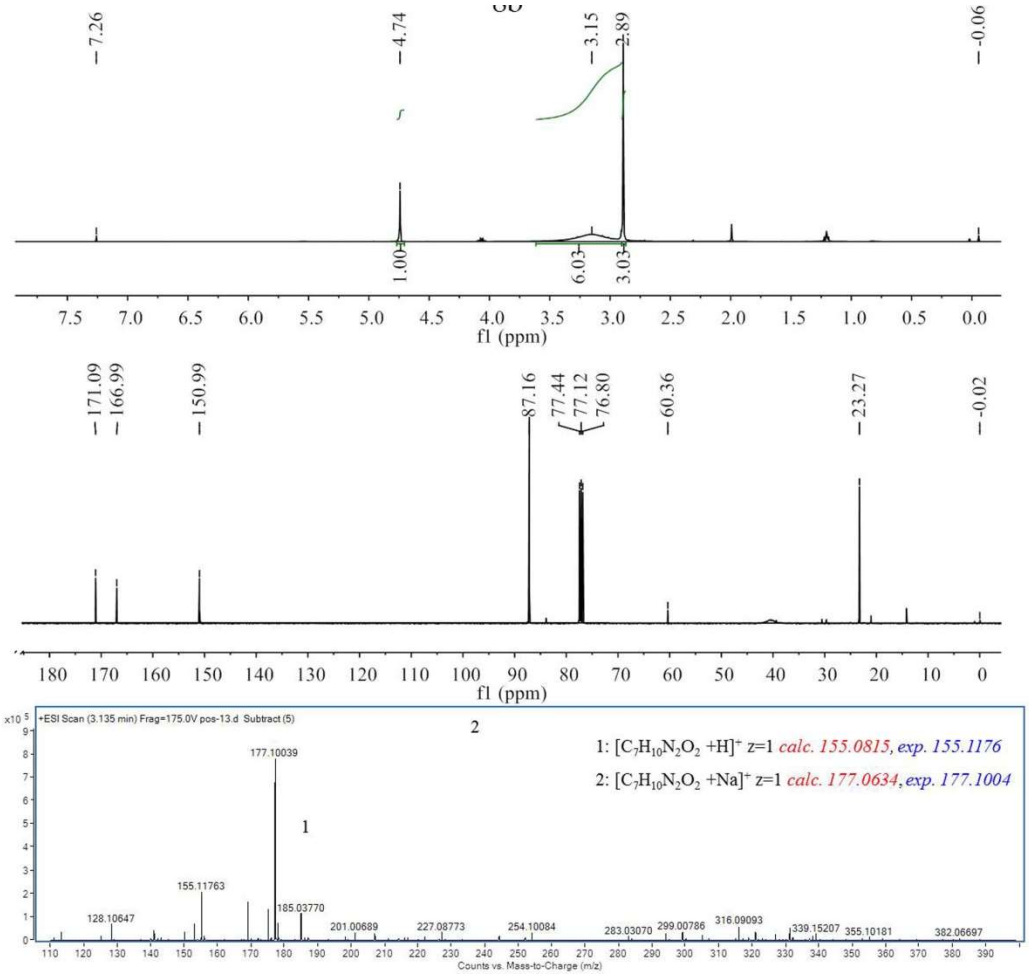

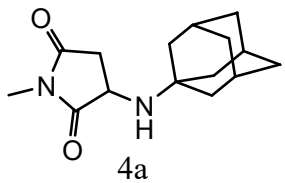

4a

4a: ^{1}H NMR (500 MHz, $CDCl_3$, ppm): δ 3.96 (dd, J = 7.7, 5.3 Hz, 1H), 2.98 (s, 3H), 2.93 (dd, J = 17.8, 9.6 Hz, 1H), 2.53 (dd, J = 17.8, 5.0 Hz, 1H), 2.09 (s, 3H), 1.85 (s, 1H), 1.69 (t, J = 11.0 Hz, 6H), 1.60 (d, J = 11.8 Hz, 3H), 1.53 (d, J = 11.1 Hz, 3H). ^{13}C NMR (126 MHz, $CDCl_3$, ppm): δ 178.36, 174.73, 50.08, 49.06, 42.11, 39.87, 35.41, 28.46, 24.09. ESI-MS for **4a**,Calcd: m/z = 263.1754 $[M+H]^+$; Found: 263.1748 $[M+H]^+$.

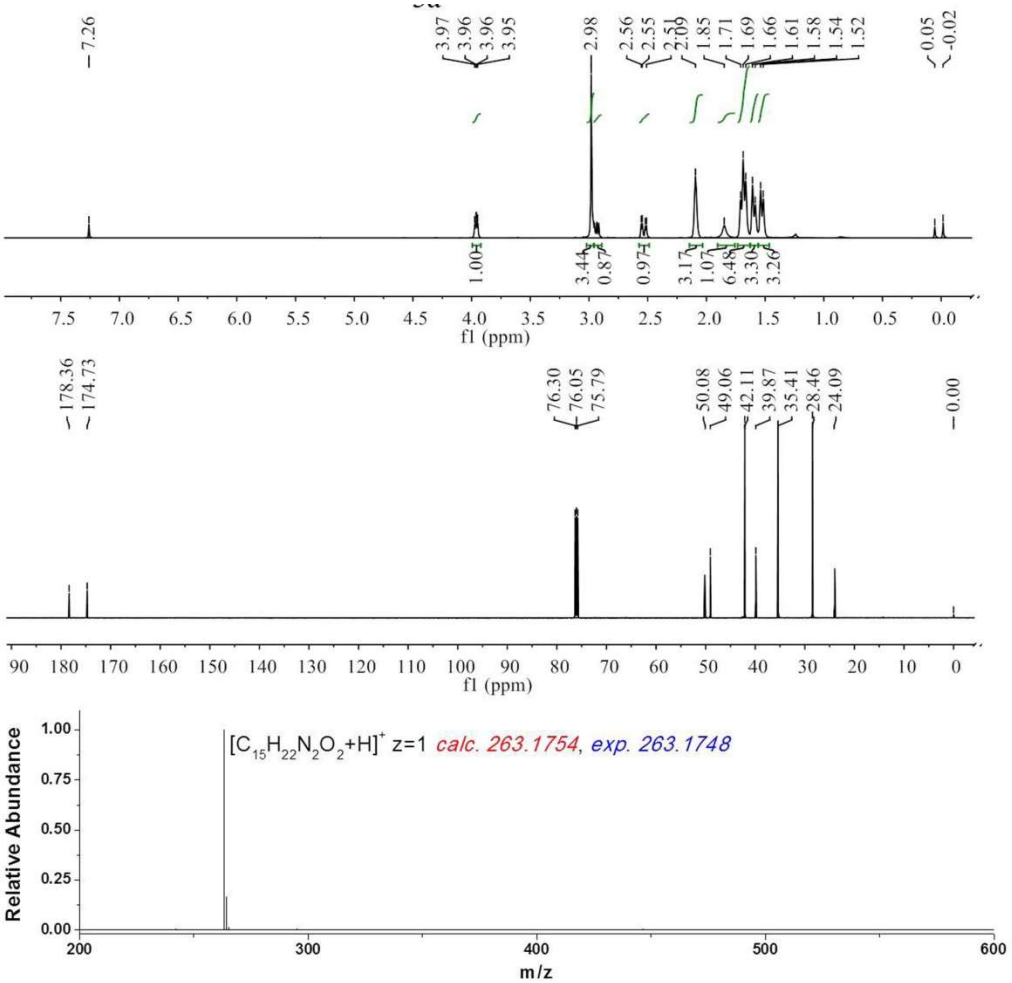

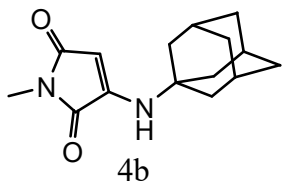

4b

4b: ^{1}H NMR (400 MHz, $CDCl_3$, ppm): δ 5.37 (s, 1H),4.79 (s, 1H), 3.16 (dd, J = 13.1, 7.0 Hz, 2H), 2.96 (s, 3H), 1.66 – 1.57 (m, 2H), 1.39 (dq, J =14.6, 7.3 Hz, 2H), 0.94 (t, J = 7.3 Hz, 3H), ^{13}C NMR (101 MHz, $CDCl_3$, ppm): δ 172.69, 167.66, 149.49, 83.83, 44.01, 30.55, 23.45, 20.00, 13.66. ESI-MS for **4b**,$[M+H]^+$Calcd: m/z = 261.1598; Found: 261.1590; $[M+Na]^+$ Calcd: m/z = 283.1417; Found: 269.1409; $[M+K]^+$ Calcd: m/z = 299.1156, Found: 285.1150.

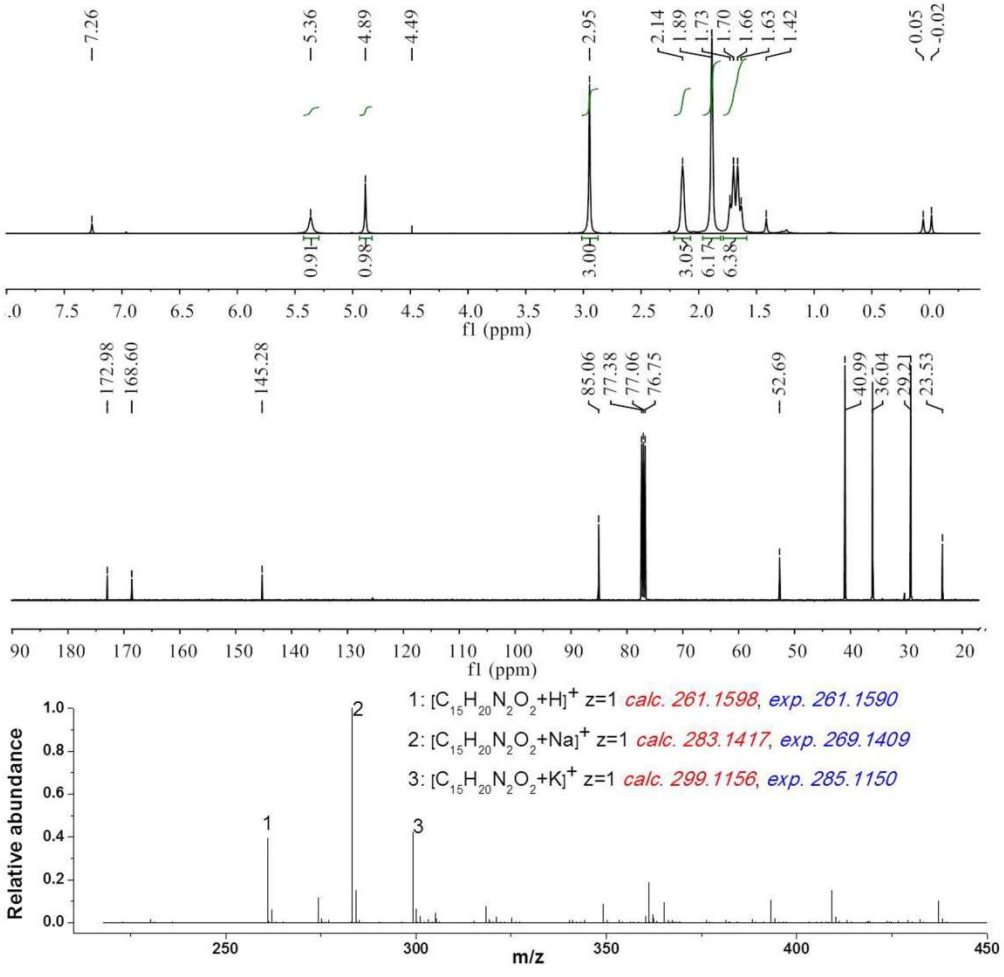

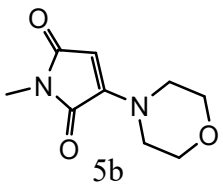

5b

5b: ^{1}H NMR (400 MHz, $CDCl_3$, ppm): δ 4.94 (s, 1H), 3.78 (dd, J = 5.8, 3.9 Hz, 4H), 3.68 (s, 4H), 2.95 (s, 3H), ^{13}C NMR (101 MHz, $CDCl_3$, ppm): δ 170.87, 167.34, 150.27, 89.84, 66.31, 23.39. ESI-MS for **5b**, $[M+H]^+$ Calcd: m/z = 197.1285; Found: 197.1274.

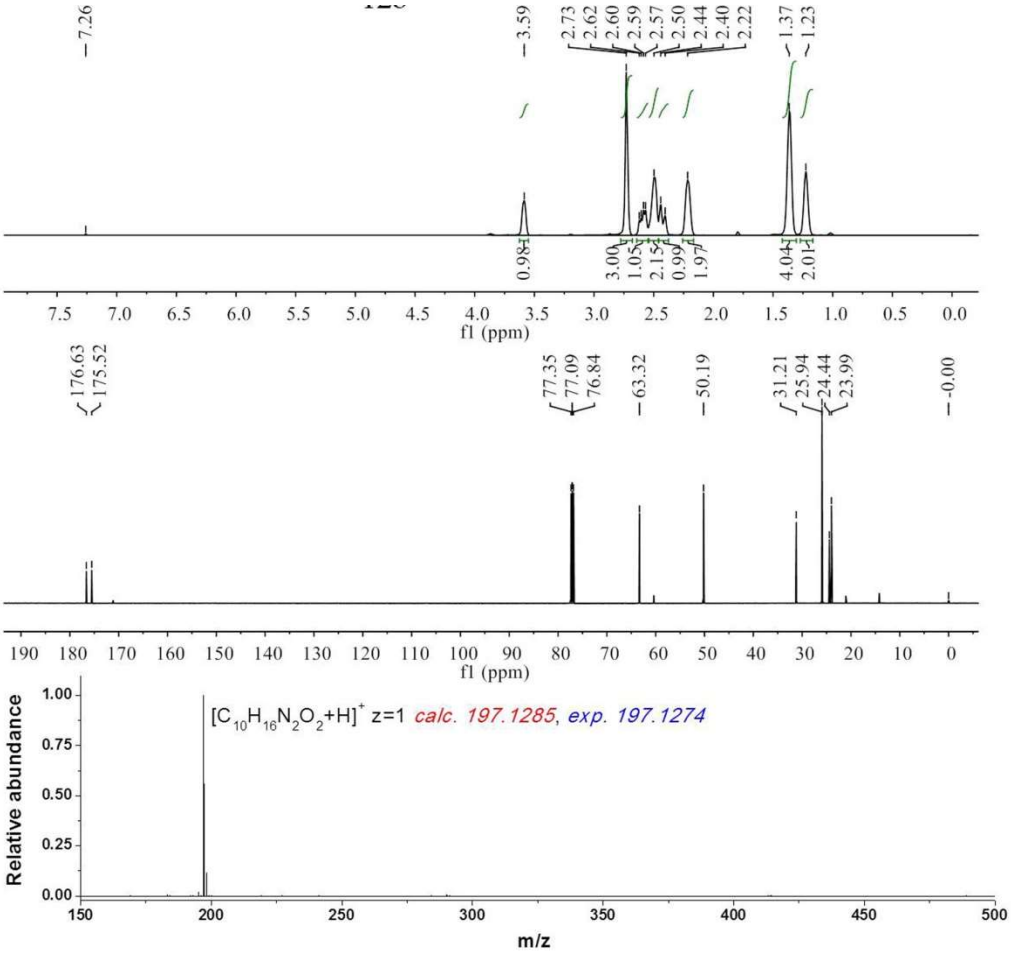

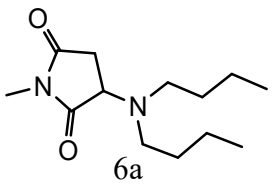

6a

6a: ^{1}H NMR (501 MHz, $CDCl_3$, ppm): δ 3.95 (dd, *J* = 8.6, 5.2 Hz, 1H), 2.94 (s, 3H), 2.77 (dd, *J* = 18.4, 9.0 Hz, 1H), 2.60 – 2.47 (m, 3H), 2.42 – 2.32 (m, 2H), 1.40 (s, 4H), 1.26 (dd, *J* = 14.6, 7.2 Hz, 4H), 0.86 (t, *J* = 7.3 Hz, 6H), ^{13}C NMR (126 MHz, $CDCl_3$, ppm): δ 177.70, 175.65, 77.26, 77.06, 76.80, 59.59, 50.95, 32.03, 30.43, 24.48, 20.41, 13.99. ESI-MS for **6a**, $[M+H]^+$Calcd: m/z = 241.1911; Found: 241.1893.

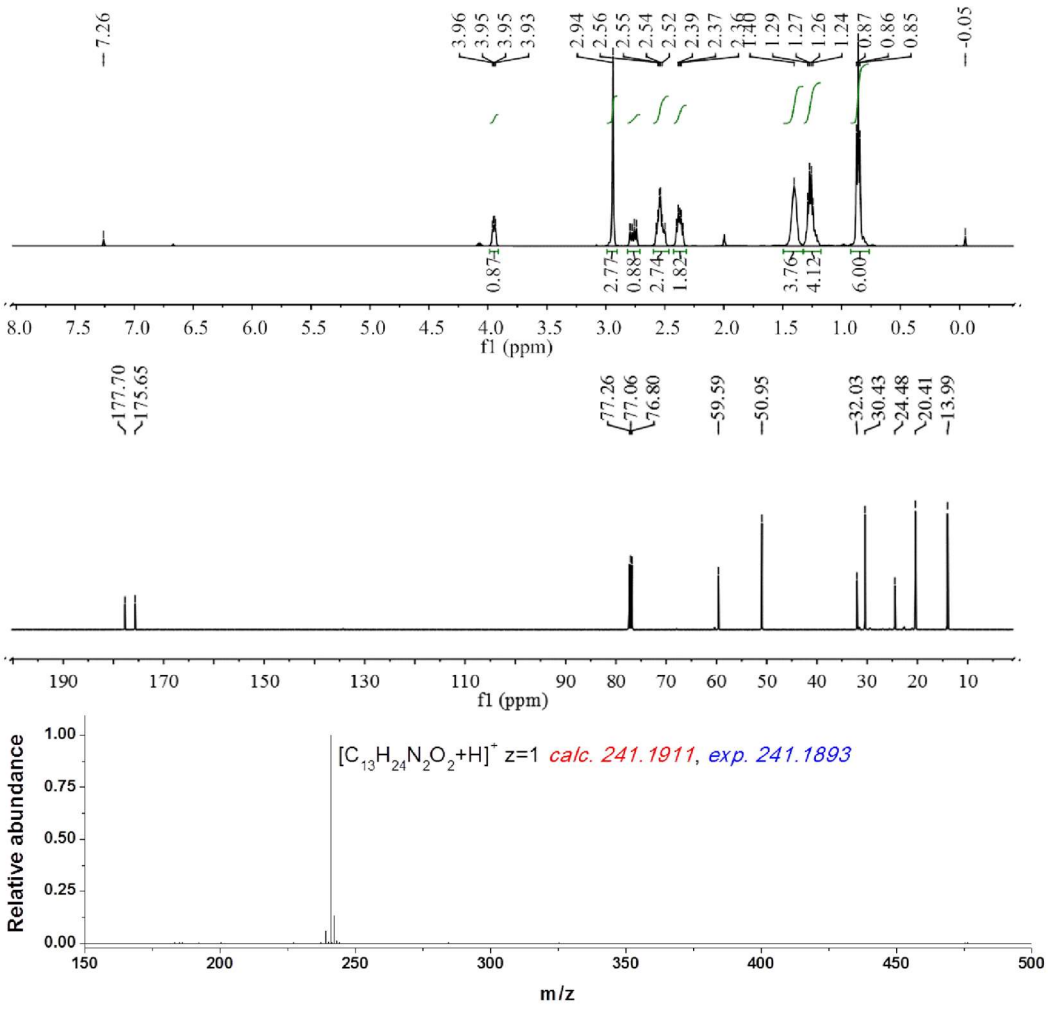

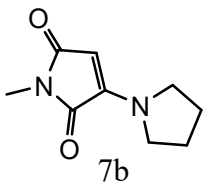

7b

7b: ^{1}H NMR (400 MHz, $CDCl_3$, ppm): δ 4.67 (s, 1H), 3.84 (s, 2H), 3.24 (s, 2H), 2.92 (s, 3H), 1.95 (s, 4H), ^{13}C NMR (101 MHz, $CDCl_3$, ppm): δ 170.89, 165.87, 147.61, 84.49, 49.18, 47.89, 25.27, 23.04, 22.24. ESI-MS for **7b**, $[M+H]^+$ Calcd: m/z = 181.0978; Found: 181.0972; $[M+Na]^+$ Calcd: m/z = 203.0791; Found: 203.0974.

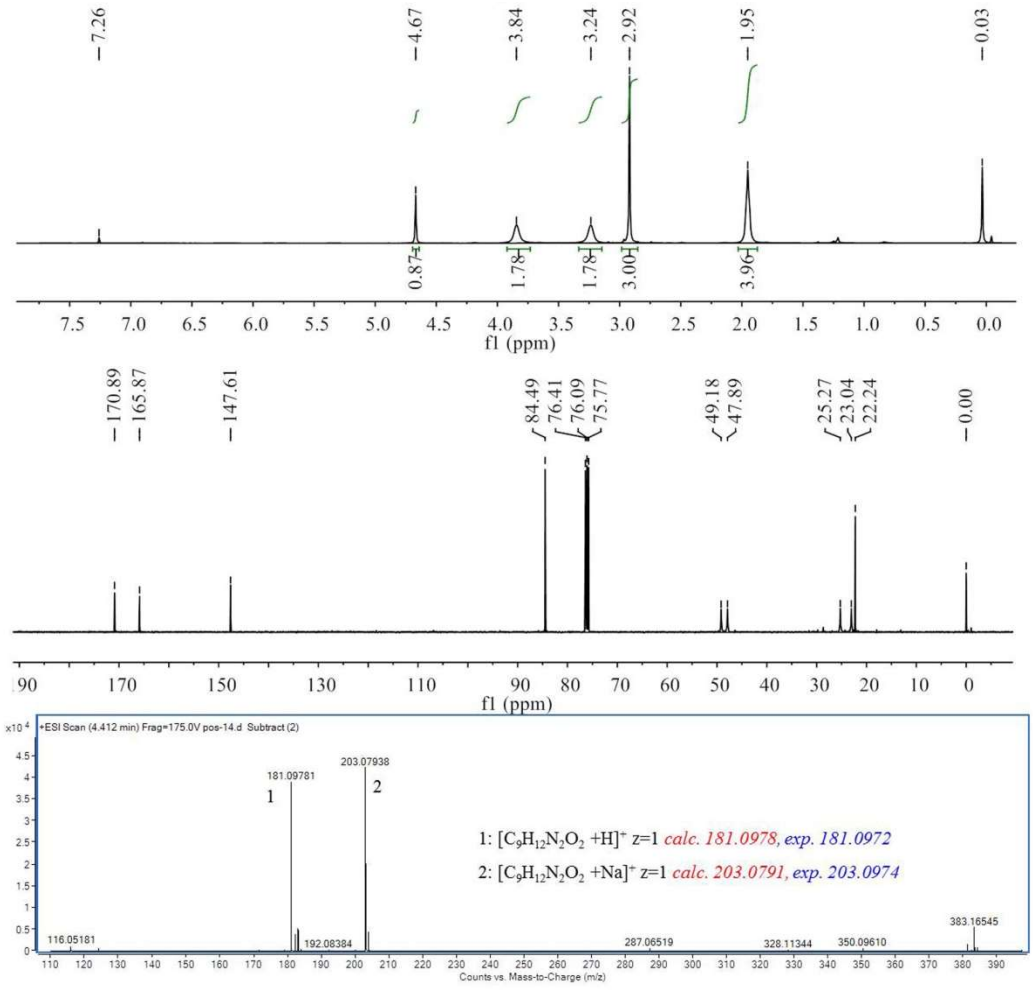

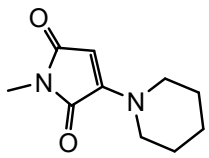

8b

8b:^{1}H NMR (400 MHz, $CDCl_3$, ppm): δ 4.84 (s, 1H), 3.62 (s, 4H), 2.91 (s, 3H), 1.64 (s, 6H), ^{13}C NMR (101 MHz, $CDCl_3$, ppm): δ 171.21, 167.43, 150.57, 87.84, 48.49, 25.61, 23.99, 23.29. ESI-MS for **8b**,$[M+H]^+$ Calcd: m/z = 195.1128; Found: 195.1142; $[M+Na]^+$ Calcd: m/z = 217.0947; Found: 217.0930.

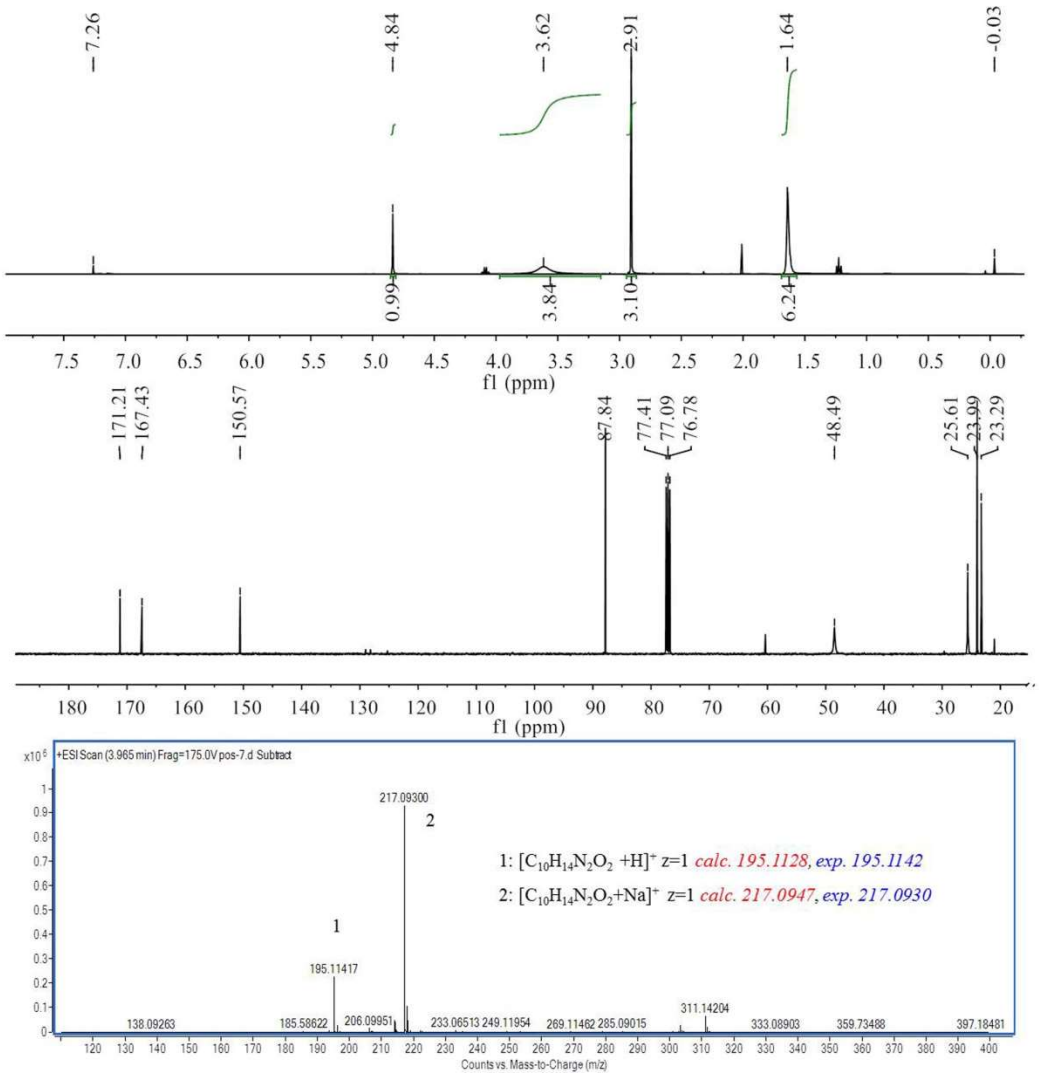

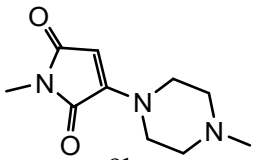

9b

9b: ^{1}H NMR (400 MHz, $CDCl_3$, ppm): δ 4.90 (s, 1H), 2.93 (s, 3H), 2.53 – 2.47 (m, 4H), 2.32 (s, 3H), 2.03 (s, 2H), 1.24 (t, J = 7.1 Hz, 2H), ^{13}C NMR (101 MHz, $CDCl_3$, ppm): δ 171.04, 167.39, 150.28, 89.30, 54.34, 46.45, 23.38. ESI-MS for **9b**,$[M+H]^+$ Calcd: m/z = 210.1237; Found: 210.1240.

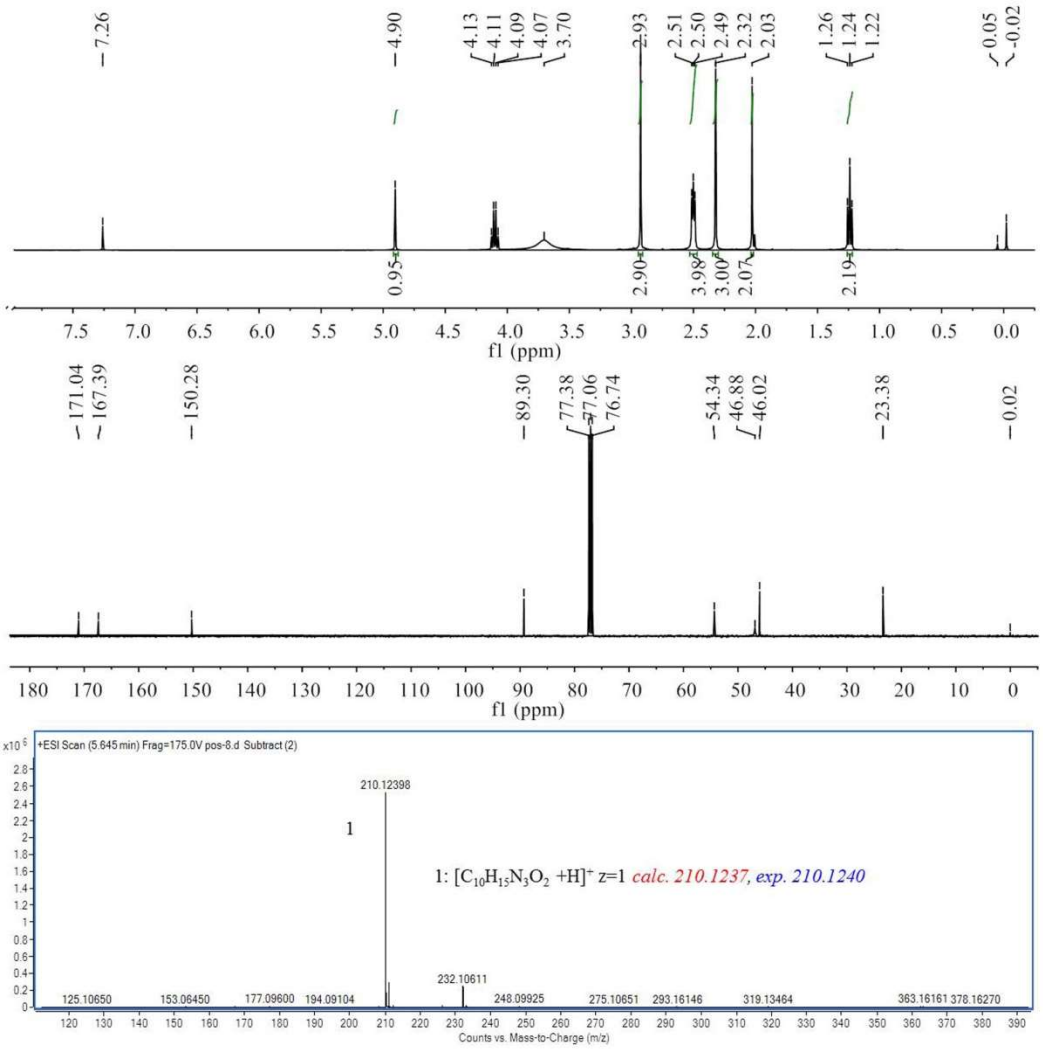

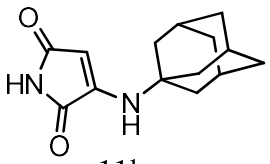

11b

11b: ^{1}H NMR (400 MHz, DMSO, ppm): δ 10.21 (s, 1H), 6.54 (s, 1H), 4.97 (s, 1H), 2.05 (s, 3H), 1.85 (d, J = 14.5 Hz, 6H), 1.63 (q, J = 12.4 Hz, 6H), ^{13}C NMR (101 MHz, $CDCl_3$, ppm): δ 170.87, 167.34, 150.27, 89.84, 66.31, 47.50, 23.39. ESI-MS for **11b**,$[M+H]^+$ Calcd: m/z = 247.1441; Found: 247.1435; $[M+Na]^+$ Calcd: m/z = 269.1260; Found: 269.1246; $[M+K]^+$ Calcd: m/z = 285.0999; Found: 285.0985.

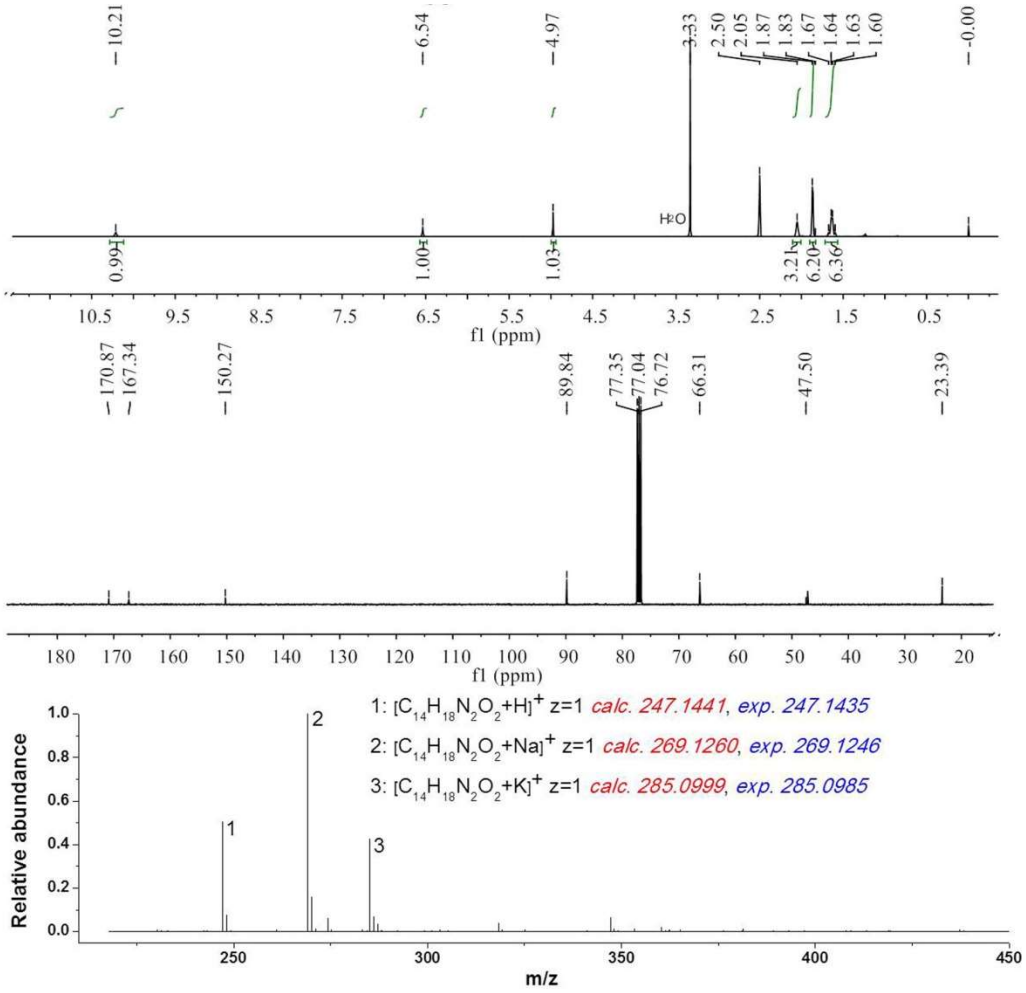

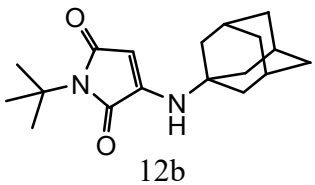

12b

12b: ^{1}H NMR (400 MHz, $CDCl_3$, ppm): δ 5.25 (s, 1H), 4.78 (s, 1H), 2.13 (s, 3H), 1.86 (s, 6H), 1.68 (q, J = 12.2 Hz, 6H), 1.56 (s, 9H), ^{13}C NMR (101 MHz, $CDCl_3$, ppm): δ 173.49, 168.23, 143.15, 84.68, 55.70, 51.27, 40.04, 35.05, 28.15. ESI-MS for **12b**,$[M+H]^+$ Calcd: m/z = 303.2067; Found: 303.2052; $[M+Na]^+$ Calcd: m/z = 325.1886; Found: 325.1866; $[M+K]^+$ Calcd: m/z = 341.1626; Found: 341.1610.

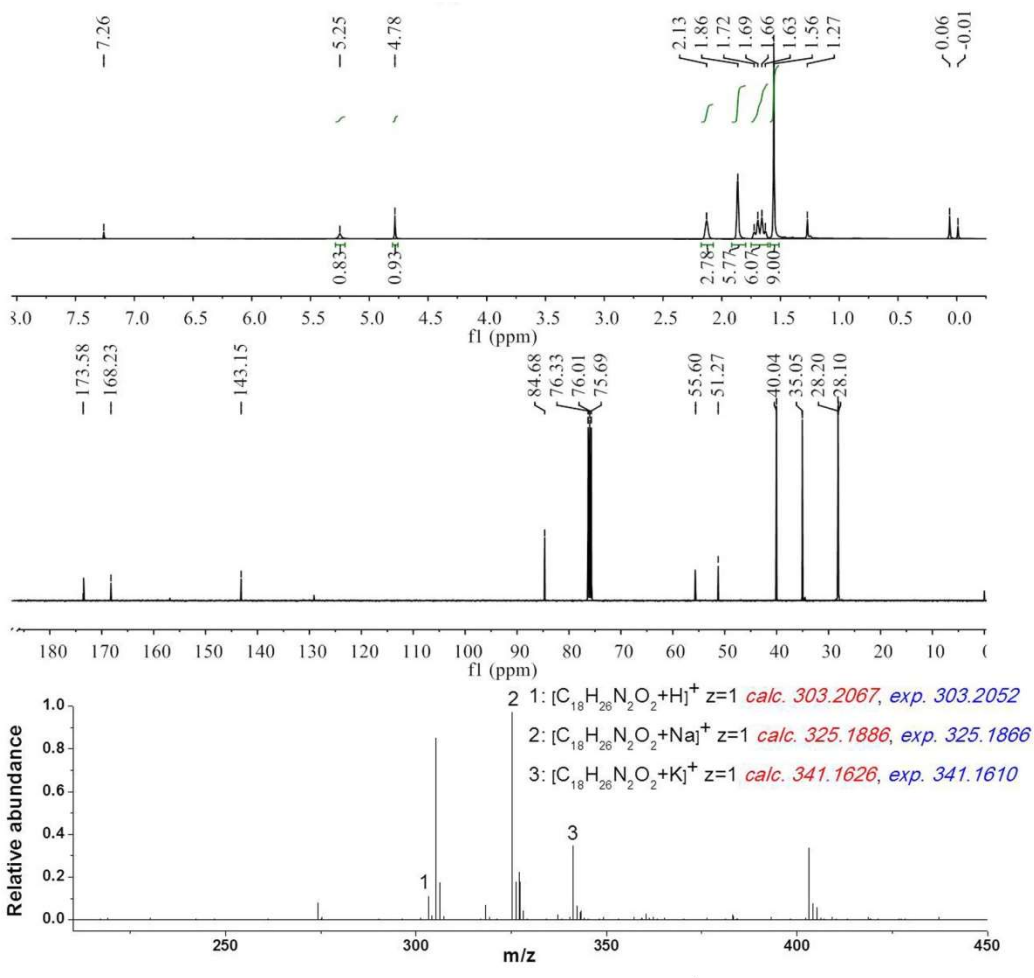

The author contributions

H.-X. Wang and H.-L. Zhang initiate the project collaboratively. H.-X. Wang conceived and designed the experiments. Y. Guo, L. Yao, and Z. Yang performed the experiments and analyzed the data. L. Luo and Y. Zhang performed the theoretical calculations. S.-L. Ai performed the cell labeling experiments. H.-X. Wang wrote the manuscript, and all the authors discussed and revised it together.

Reference

[1] M. J. Frisch, G. W. Trucks, H. B. Schlegel, G. E. Scuseria, M. A. Robb, J. R. Cheeseman, G. Scalmani, V. Barone, G. A. Petersson, H. Nakatsuji, X. Li, M. Caricato, A. V. Marenich, J. Bloino, B. G. Janesko, R. Gomperts, B. Mennucci, H. P. Hratchian, J. V. Ortiz, A. F. Izmaylov, J. L. Sonnenberg, D. Williams-Young, F. Ding, F. Lipparini, F. Egidi, J. Goings, B. Peng, A. Petrone, T. Henderson, D. Ranasinghe, V. G. Zakrzewski, J. Gao, N. Rega, G. Zheng, W. Liang, M. Hada, M. Ehara, K. Toyota, R. Fukuda, J. Hasegawa, M. Ishida, T. Nakajima, Y. Honda, O. Kitao, H. Nakai, T. Vreven, K. Throssell, J. A. Montgomery, Jr., J. E. Peralta, F. Ogliaro, M. J. Bearpark, J. J. Heyd, E. N. Brothers, K. N. Kudin, V. N. Staroverov, T. A. Keith, R. Kobayashi, J. Normand, K. Raghavachari, A. P. Rendell, J. C. Burant, S. S. Iyengar, J. Tomasi, M. Cossi, J. M. Millam, M. Klene, C. Adamo, R. Cammi, J. W. Ochterski, R. L. Martin, K. Morokuma, O. Farkas, J. B. Foresman, and D. J. Fox, Gaussian 16, Revision A.03, Gaussian, Inc., Wallingford CT, 2016.

[2] Y. Zhang and B. Champagne, **J. Phys. Chem. C**, 2013, ***117***, 1833–1848.

[3] Y. Zhang, R. Steyrleuthner and J. L. Bredas, **J. Phys. Chem. C**, 2016, ***120***, 9671–9677.

[4] Y. F. Huang, X. Zhou, R Zhou, H. Zhang, K. B. Kang, M. Zhao, Y. Peng, Q. Wang, H. L. Zhang and W. Y. Qiu, **Eur. Chem. J**., 2014, ***20***, 5640-5648.

[5] Y. Tang, T. Yang, Q. Wang, X. Lv, X. Song, H. Ke, Z. Guo, X. Huang, J. Hu, Z. Li, P. Yang, X. Yang and H. Chen, **Biomaterials**, 2018, ***154***, 248-260.

[6] Y. Tao, S. Peng, X. D. Wang, Z. Z. Li, X. J. Zhang, and L. S. Liao, **Adv. Funct. Mater**., 2018, ***28***, 1804915.

[7] Y. Wang, G. Zhang, W. Zhang, X. D. Wang, Y. Wu, T. Liang, X. Hao, H. Fu, Y. Zhao, and D. Zhang, **Small**, 2016, ***12***, 6554-6561.

[8] J. Bergman and T. Brimert, **Acta Chem. Scand.**, 1999, ***53***, 48-56.